Coastal deformation and great subduction earthquakes, Isla Santa María, Chile (37°S)

Daniel Melnick[†]
GeoForschungsZentrum Potsdam, Telegrafenberg, 14473 Potsdam, Germany, and *Institut für Geowissenschaften, Universität Potsdam, Postfach 601553, 14415 Potsdam, Germany*

Bodo Bookhagen[‡]
Department of Geological Sciences, University of California, Santa Barbara, California 93106, USA, and *Institut für Geowissenschaften, Universität Potsdam, Postfach 601553, 14415 Potsdam, Germany*

Helmut P. Echtler
GeoForschungsZentrum Potsdam, Telegrafenberg, 14473 Potsdam, Germany

Manfred R. Strecker
Institut für Geowissenschaften, Universität Potsdam, Postfach 601553, 14415 Potsdam, Germany

ABSTRACT

Isla Santa María at the active margin of south-central Chile is the result of earthquake-related uplift and deformation in the forearc since at least late Pleistocene time. Field mapping, dating of key depositional horizons, and analysis of seismic-reflection profiles reveal ongoing deformation in this sector of the Chilean forearc. The 30 km² island is located ~12 km above the interplate seismogenic zone and 75 km landward of the trench. It is situated near the southern termination of the Concepción earthquake rupture segment, where Charles Darwin measured 3 m of coseismic uplift during a M > 8 megathrust earthquake in 1835. Permanent postearthquake deformation from this earthquake and an earlier event in 1751 is registered by emerged, landward-tilted abrasion surfaces. Uplift at ~2 m/k.y. and tilting at ~0.025°/k.y. of the island have been fairly constant throughout the late Quaternary and have resulted in emergence of the island above sea level ~31 k.y. ago. The island is composed of a late Pleistocene upper, tilted surface with two asymmetric tilt domains, and Holocene lowlands characterized by uplifted and tilted strandlines. Industry offshore seismic-reflection profiles covering an area of ~1800 km² and crustal seismicity reveal active reverse-fault cored anticlines surrounding Isla Santa María; the principal fault apparently roots in the plate-interface thrust. These reverse faults in the upper plate result from inversion of late Cretaceous to early Pliocene normal faults and rift structure of the Arauco forearc basin. Positive inversion of these inherited structures started between 3.6 and 2.5 Ma and resulted in continuous shortening rates of ~0.8 mm/yr. The seismic-reflection profiles show that the asymmetric tilt domains and progressive syntectonic sedimentation are linked to the position of the island in the fore-limbs of two converging anticlines, whereas their backlimbs have been removed by cliff retreat. The 2 m uplift contour of the 1835 earthquake is parallel to the strike of active faults and antiforms in the Arauco-Concepción region. The close relation among the asymmetric uplift and tilt of the island, modern deformation patterns, and reverse faults rooted in the plate interface suggests that slip on the plate interface thrust influences, localizes, and segments surface deformation during large interplate earthquakes. Furthermore, the link between positive inversion of pre-existing structures, uplift, and tilt patterns in the forearc emphasizes the importance of inherited structural fabrics in guiding plate-boundary deformation.

Keywords: Chile margin, forearc deformation, subduction earthquakes, tectonic inversion, reverse faults, crustal seismicity.

[†]Corresponding author e-mail: melnick@gfz-potsdam.de.
[‡]Present address: Department of Geological and Environmental Sciences, Stanford University, Stanford, California 94305, USA.

INTRODUCTION

Uplift and subsidence are first-order phenomena of tectonically active coasts along subduction margins (e.g., Plafker, 1972; Ando, 1975). Emergent coasts are usually characterized by differential uplift within distinct segments that may be sustained as morphotectonic units on time scales of 10^5 to 10^6 yr. During earthquakes, these areas appear to act as semi-independent rupture zones that guide deformation (e.g., Kaizuka et al., 1973; Ando, 1975; Matsuda et al., 1978; Taylor et al., 1987; Thatcher, 1990; Berryman, 1993b; Pandolfi et al., 1994; Ota and Yamaguchi, 2004). Coseismic land-level changes caused by subduction earthquakes follow a sinusoidal deformation pattern across the margin, with uplift along the shelf and coast, and subsidence farther inland (e.g., Plafker and Savage, 1970; Savage, 1983; Hyndman and Wang, 1995). This idealized distribution of coseismic deformation is dramatically altered, however, when pre-existing faults in the upper plate are triggered by a megathrust event, such as during the M 9.2 Alaskan earthquake in 1964 (Plafker, 1972). In some subduction zones, crustal faults have controlled coastal deformation patterns and forearc basin formation over million-year time scales, and their subdivisions seem to govern seismotectonic segmentation, rupture propagation, and susceptibility to local earthquake hazards (e.g., Berryman et al., 1989; Goldfinger et al., 1992; Barnes et al., 2002; Johnson et al., 2004; Bruhn and Haeussler, 2006; Briggs et al., 2006). Some of these faults are rooted in the plate-interface thrust, and mechanical coupling

with the megathrust during the earthquake cycle is thus expected (e.g., Park et al., 2000; Barnes et al., 2002; Bruhn and Haeussler, 2006).

This study focuses on the Chile active margin, which is composed of distinct coastal segments undergoing long-term differential uplift and subsidence manifested in a rich array of coastal landforms. Historic accounts of great subduction earthquakes in Chile indicate the protracted existence of discrete rupture segments (Lomnitz, 1970, 2004; Kelleher, 1972; Nishenko, 1985; Comte et al., 1986; Thatcher, 1990; Beck et al., 1998). Figure 1A shows the southern segments. However, it is not known over what time scales these rupture segments prevail and what their influence is with respect to overall landscape development. We present the deformation history for Isla Santa María in the south-central Chile margin (Fig. 1A), where continuous late Quaternary uplift and tilting are recorded in the geomorphology and coastal deposits of this island, which experienced meter-scale coseismic uplift during the last great interplate earthquake (Fig. 2C). The island is located near the transition between two distinct seismotectonic sectors, the Concepción and Valdivia segments (Fig. 1A). We use detailed geologic mapping, stratigraphy, geomorphology, and radiocarbon dating to demonstrate that the island is being differentially uplifted and tilted. Furthermore, we analyze seismic-reflection profiles and crustal seismicity patterns to show that active reverse faults rooted in the plate interface have been responsible for the progressive uplift and tilting of this island. Our results demonstrate that morphotectonic segmentation along this part of the Chile margin is fundamentally controlled by inverted crustal-scale faults, therefore highlighting the importance of structural inheritance in tectonically active regions.

METHODS AND DATA SOURCES

For geological mapping and geomorphic analysis of Isla Santa María, we used aerial photos at a scale of 1:20,000 and a photogrammetrically derived digital elevation model at 5 m resolution (Fig. 3). Detailed stratigraphic sections were surveyed and sampled at sea-cliff exposures, which allowed us to measure the elevation of the Tertiary–Pleistocene unconformity at 80 locations. Fourteen accelerator mass spectrometry (AMS) radiocarbon ages were obtained from wood and charcoal collected in paleosols, peat, and clay layers from the Pleistocene units and Holocene debris-flow deposits (Table 1). The ages were calibrated with the Calpal software (www.calpal.de) using the *Calpal 2004 January* calibration curve (Stuiver et al., 1998; Hughen et al., 2004). We believe that the sampled material is uncontaminated because of: (1) stratigraphic concordance—ages of lower stratigraphic levels are older; (2) thickness of the sedimentary sequence—the samples were taken from fresh sea-cliff exposures where no roots or other exotic material was present, several meters below the top of the sequence; and (3) the type of material—dating was performed on centimeter-size charcoal and large pieces of well-preserved wood.

Tectonic uplift rates were calculated using the radiocarbon ages and the sea-level curve from Siddall et al. (2003). Uplift rates derived from optically stimulated luminescence ages of late Holocene strandlines and a detailed topographic survey based on measurements with a laser theodolite are presented in Bookhagen et al. (2005) and Bookhagen et al. (2006). Active structures offshore were interpreted from migrated seismic-reflection profiles provided by Empresa Nacional del Petróleo (ENAP, the Chilean state oil company) (Fig. 2C), and crustal seismicity data recorded by the ISSA (Integrated Seismological experiment in the Southern Andes) local network (Fig. 2D). The seismic stratigraphy was correlated with ENAP exploration boreholes and outcrops in the Arauco Bay area (Figs. 2C and 2A) (Mordojovich, 1981; González, 1989; Vietyes et al., 1993; Elgueta and Arcos, 1994). The ISSA data were collected during a three-month-long experiment using 62 broadband instruments and 16 ocean bottom seismometer/hydrophone (OBH/OBS) deployed between 36 and 40°S (Bohm et al., 2002; Bruhn, 2003).

REGIONAL TECTONIC AND GEOLOGIC SETTING

The Chile margin is formed by subduction of the Nazca plate under the South American continent, at a convergence rate of ~80 mm/yr averaged for the past ~3 m.y. (Somoza, 1998) or 66 mm/yr determined from global positioning system (GPS) modeling (Angermann et al., 1999). The Juan Fernández Ridge and Chile Rise constitute major bathymetric anomalies and tectonic discontinuities of the Nazca plate, and are located to the north and south of the study area, respectively (Fig. 1A). At 37°S, seismic-reflection profiles image a filled trench with up to 2.2 km of turbidites and a small accretionary wedge (Fig. 1C). Part of the trench fill is frontally accreted to the margin, while the rest is underthrust into a subduction channel (Bangs and Cande, 1997). The top of the subducting Nazca plate lies at ~12–20 km depth below the shelf and coastal region where it dips ~10° eastward (Krawczyk et al., 2003).

The onshore area consists of four main morphotectonic units (Fig. 1B): (1) the Coastal Platform, formed by uplifted Cenozoic marine and continental sediments, which are the focus of this paper; (2) the Coastal Cordillera, a Paleozoic accretionary complex and magmatic arc constituting the crystalline continental basement; (3) the Central Depression, a low-lying basin filled by Pliocene-Quaternary conglomerates; and (4) the Main Cordillera, characterized by high topography and an active volcanic arc (e.g., Mpodozis and Ramos, 1989).

Isla Santa María is in the Coastal Platform, part of the Arauco Basin, a late Cretaceous to Quaternary forearc depocenter filled with at least 3.1 km of marine and continental sediments, as revealed by ENAP exploration wells (Mordojovich, 1981; González, 1989; Elgueta and Arcos, 1994). The Arauco Basin contains the Campanian to Maastrichtian Quiriquina Formation, the Paleocene to Eocene Lebu Group, the late Miocene to early Pliocene Ranquil Formation, and the late Pliocene to Pleistocene Tubul Formation (e.g., Biró, 1979; Pineda, 1986; Elgueta and Arcos, 1994; Le Roux and Elgueta, 1997; Finger et al., 2006) (Fig. 2A). Hydrocarbon exploration models of forearc basins in Chile between 34 and 45°S, supported by structural data from coal mines in the Arauco Basin, suggest that various phases of subsidence and extension occurred between the Late Cretaceous and early Pliocene (Mordojovich, 1981; González, 1989; Melnick and Echtler, 2006). Normal faults associated with these basins apparently reactivated inherited fabrics of the Paleozoic metasedimentary basement (González, 1989). In this study and in Melnick and Echtler (2006), we show that inversion of the Arauco rift basin started between 3.6 and 2.5 Ma, and that shortening has been continuous at relatively low rates during deposition of the late Pliocene to Pleistocene Tubul Formation and is active today.

Only a few previous studies have addressed late Quaternary and historic deformation along the south-central Chile margin. The pioneer work of Kaizuka et al. (1973) and detailed study by Nelson and Manley (1992) reported Holocene uplift rates between 5.5 and 10 m/k.y. at Mocha Island (Fig. 1A), based on ^{14}C ages of emerged strandlines. Marine terraces of the Arauco Peninsula and surroundings were described by Kaizuka et al. (1973) as three sequences of uplifted Pleistocene marine surfaces containing shallow-marine deposits, fluvial conglomerates, and eolian sands. These surfaces are folded around a northwest-oriented anticline in the center of the peninsula (Figs. 1B and 2A). Based on its width and lateral extension, Kaizuka et al. (1973) inferred that the broadest surface, the Cañete surface, was formed during the last interglacial sea-level highstand ca. 125 ka, and the upper two
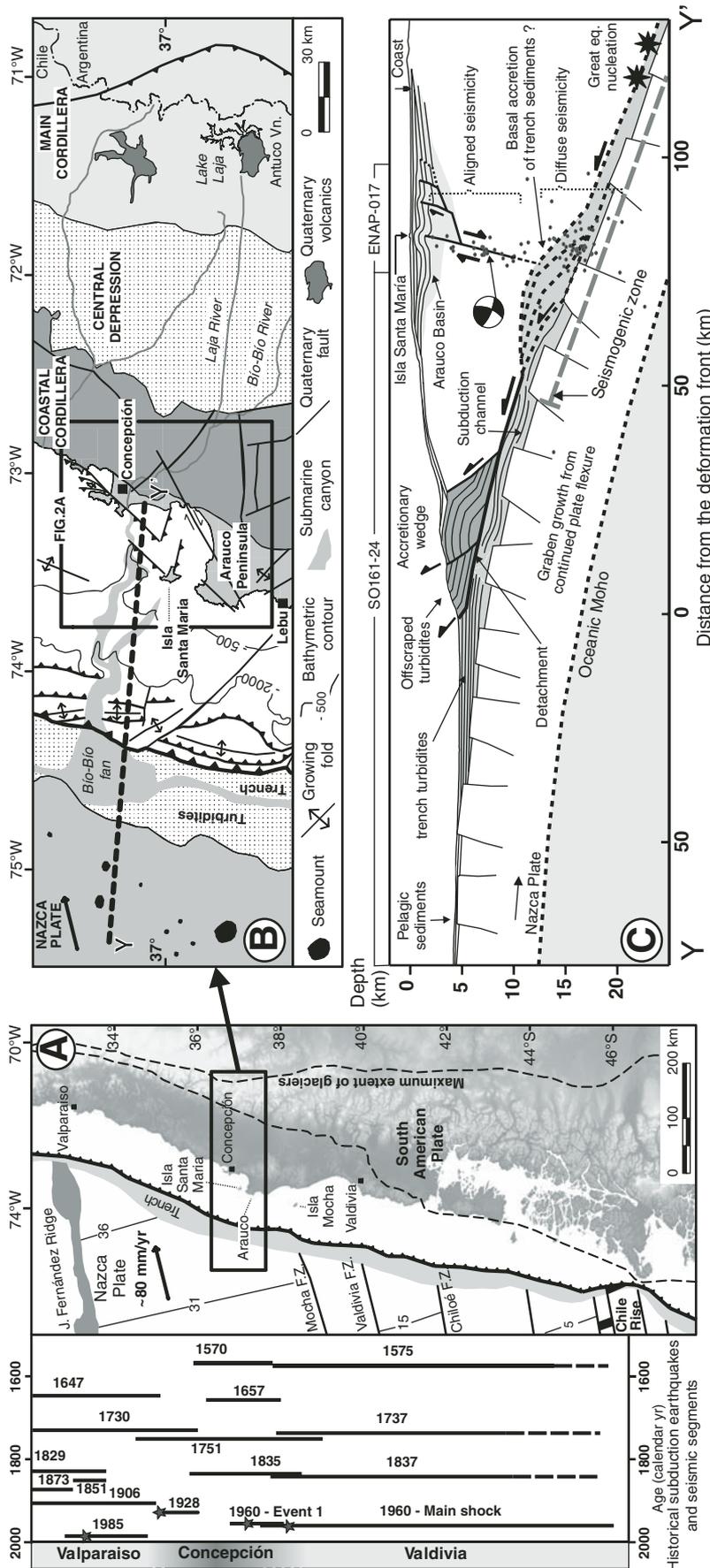
Figure 1. (A) Seismotectonic segments, rupture zones of historical subduction earthquakes, and main tectonic features of the south-central Andean convergent margin. Earthquakes were compiled from Lomnitz (1970, 2004), Kelleher (1972), Comte et al. (1986), Cifuentes (1989), Beck et al. (1998), and Campos et al. (2002). Nazca plate and trench are from Bangs and Cande (1997) and Tebbens and Cande (1997). Maximum extension of glaciers is from Rabassa and Clapperton (1990). F.Z.—fracture zone. (B) Regional morphotectonic units, Quaternary faults, and location of the study area. Trench and slope have been interpreted from multibeam bathymetry and seismic-reflection profiles (Reichert et al., 2002). (C) Profile of the offshore Chile margin at ~37°S, indicated by thick stippled line on the map and based on seismic-reflection profiles SO161-24 and ENAP-017. Integrated Seismological experiment in the Southern Andes (ISSA) local network seismicity (Bohm et al., 2002) is shown by dots; focal mechanism is from Bruhn (2003). Updip limit of seismogenic coupling zone from heat-flow measurements (Grevemeyer et al., 2003). Basal accretion of trench sediments from sandbox models (Lohrmann, 2002; Glodny et al., 2005). Convergence parameters from Somoza (1998).

Figure 2. Regional geology, structures, and geophysical data sets of the Arauco-Concepción region. (A) Simplified geologic map compiled from Pineda (1986), Elgueta and Arcos (1994), and personal field observations. Offshore structures were interpreted from Empresa Nacional del Petróleo (ENAP) seismic profiles. Bathymetric contours are from (Reichert et al., 2002). (B) Measurements of coseismic uplift during the 20 February 1835, M ~ 8.25 subduction earthquake from Darwin (1839). Note that the 2 m uplift contour derived from these data is parallel to the northeast-striking reverse fault system as well as the en echelon arrangement formed by Isla Quiriquina and the Hualpén, Tumbes, and Coliumo peninsulas. Shaded-relief digital elevation model (DEM) is from Shuttle Radar Topography Mission (SRTM) data. (C) ENAP seismic-reflection profiles and boreholes used in this study. Late Pliocene to Quaternary offshore structures were interpreted from these data. (D) Depth-coded seismicity is from the Integrated Seismological experiment in the Southern Andes (ISSA) local network (Bohm et al., 2002). Black focal mechanisms are from ISSA data (Bruhn, 2003), gray focal mechanism, from the U.S. Geological Survey National Earthquake Information Center (USGS-NEIC) catalogue (21 May 1990, M_w = 6.3, 5 km depth). Bathymetric contours in meters are from Pineda (1999).
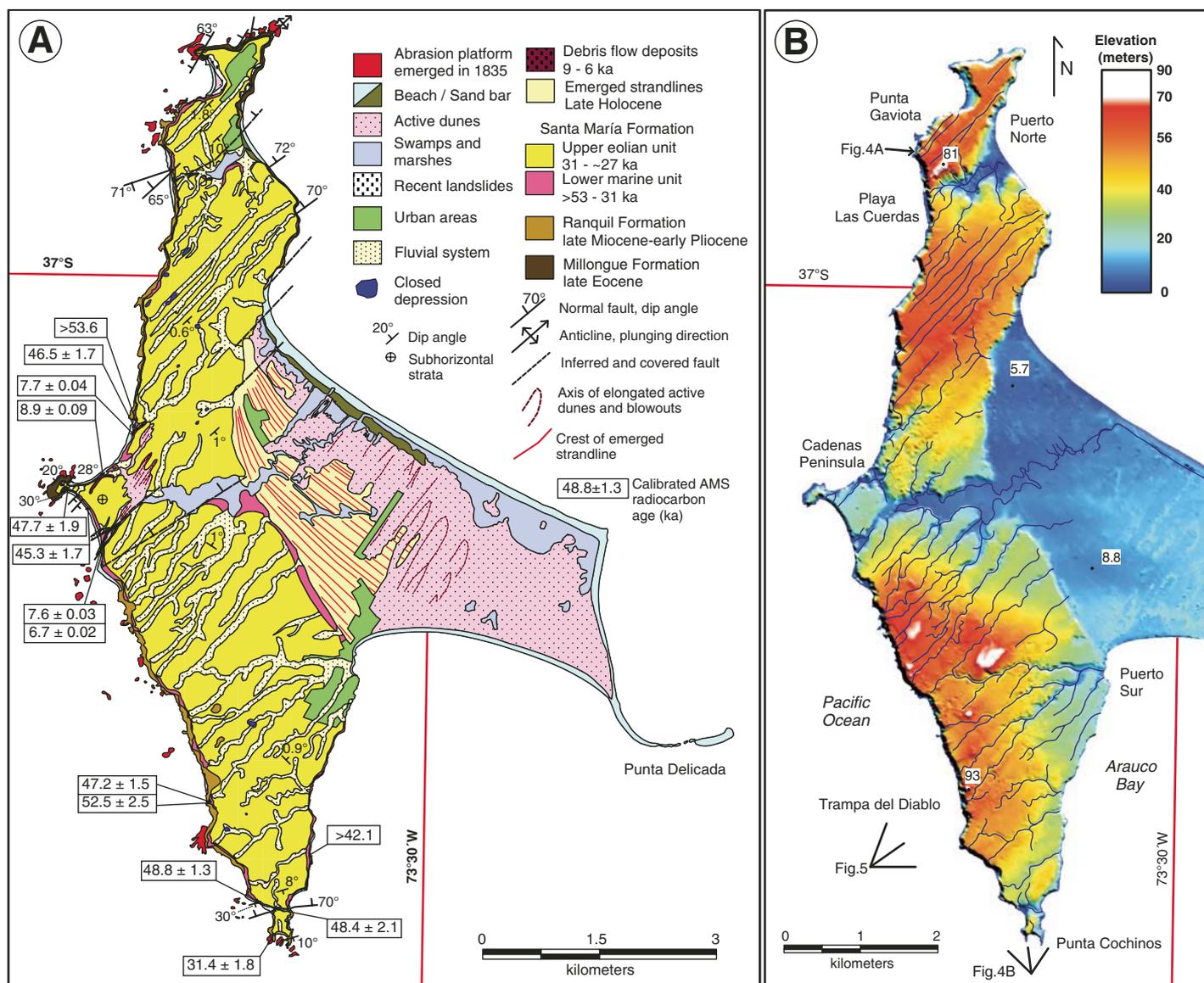

Figure 3. (A) Geologic and geomorphic map of Isla Santa María and calibrated ^{14}C ages. AMS—accelerator mass spectrometry. (B) Shaded-relief digital elevation model (5 m horizontal resolution, derived from photogrammetric restitution of 1:20,000 aerial photos) and drainage network. Labels indicate elevations in meters.

TABLE 1. RADIOCARBON AGES OBTAINED BY ACCELERATOR MASS SPECTROMETRY (AMS) DATING OF CHARCOAL AND LARGE
PIECES OF WOOD OF THE SANTA MARÍA FORMATION

Lab ID	Material	Stratigraphic position	Age (yr B.P.)	2σ error (yr)	Calibrated age (yr B.P.)	2σ error (yr)	Sea-level elevation (m)	Sample elevation (m)	Uplift rate (m/k.y.)	2σ error (yr)
KIA24186	Paleosol	Base eolian unit	27,380	1750	31,463	1885	–93.1	33.0	4.00	0.28
KIA25772	Paleosol	Base marine unit	47,600	1250	48,826	1318	–78	3.5	1.66	0.40
KIA24181	Paleosol	Base marine unit	52,750	2530			–46.1	12.5	1.28	0.35
KIA25771	Clay	Base marine unit	>42,130				–82	5.4	2.07	0.56
KIA24182	Peat	Base marine unit	>53,600				–68	6.0	1.38	0.44
KIA24188[†]	Clay	Int. marine unit	43,780	1500	45,319	1760	–77	3.1 + 15.3	2.10	0.39
KIA25773	Clay	Int. marine unit	44,480	725	47,250	1505	–85	24.8	2.32	0.36
KIA24190	Peat	Int. marine unit	45,450	1300	46,540	1735	–70	6.2	1.63	0.39
KIA24182	Peat	Int. marine unit	47,280	1760	47,769	1976	–78.8	5.0	1.92	0.35
KIA24187[†]	Paleosol	Int. marine unit	48,080	1900	48,442	2180	–84.8	15.0 + 20.4	2.10	0.31
KIA24178	Peat /df.	Filling channel	5890	30	6703	26		3.6		
KIA24179	Peat /df.	Filling channel	6835	40	7660	33		2.6		
KIA24189	Peat /df.	Filling channel	6900	45	7731	40		7.2		
KIA24180	Peat /df.	Filling channel	8020	35	8900	93		10.2		

Note: Dating was performed at the Leibnitz-Labor AMS facility in Kiel, Germany. Calibration was made with the Calpal software (www.calpal. de) using the *January 2004 calibration curve*. Sea-level elevations are from Siddall et al. (2003) and have a 2σ error of 12 m. The latter and the present elevation of the samples were added to obtain the uplift by assuming that the samples were deposited at, or very near to, sea level. The uplift rates are also presented in Figure 9. Int—interbedded; df.—debris-flow deposit.

[†]Beds tilted by adjacent normal growth faults and affected by postdepositional subsidence. The added elevation value has been estimated considering bed dip and distance from sampling point to half-graben hinge.

surfaces were formed during the preceding interglacial highstands. If this inference is true, an uplift rate of ~1.8 m/k.y. results for the center of the folded peninsula. Surfaces with similar nearshore deposits, but narrower, less pronounced, and lacking longitudinal continuity, exist at lower elevations in the Arauco-Concepción region, and were correlated with late Pleistocene interstadials (Kaizuka et al., 1973). Based on the rupture zones of historical earthquakes (Fig. 1A), Kaizuka et al. concluded that the Arauco Peninsula exists as a result of overlap between the Valdivia and Concepción seismic rupture zones (see section on historical earthquakes). However, the mechanistic explanation for the relation between the broad megathrust ruptures, localized folding and uplift of Pleistocene surfaces, and the general coastal geomorphology has remained unsolved.

HISTORIC EARTHQUAKES

Five hundred years of historic records of subduction earthquakes in Chile show that Isla Santa María is within the southern part of the Concepción seismic segment (Lomnitz, 1970; Barrientos, 1987; Thatcher, 1990; Beck et al., 1998; Campos et al., 2002), which nucleated M > 8 subduction earthquakes in 1570, 1657, 1751, and 1835 (Lomnitz, 1970, 2004) (Fig. 1A). Until the last event in 1835, this segment followed a rather periodic pattern with a recurrence of 88 ± 5 yr (mean ±1σ standard deviation), which is very similar to the 82 ± 7 yr recurrence interval of the Valparaiso segment immediately to the north (Comte et al., 1986), but lower than the 128 ± 31 yr recurrence interval of the Valdivia segment to the south. The 1960 seismic sequence, which produced the largest earthquake ever recorded instrumentally, started with a M_w = 8.1 foreshock that nucleated at 37°10′S, immediately north of the Arauco Peninsula with a rupture length of ~150 km (Cifuentes, 1989) (Fig. 1A). The M_w = 9.5 main shock nucleated a day after at 38°30′S and ruptured the entire Valdivia segment between 37°30′ and 46°30′S (Plafker and Savage, 1970; Kanamori, 1977; Cifuentes, 1989).

The Concepción segment is considered to be a seismic gap because it has not ruptured since 1835 (Barrientos, 1987; Campos et al., 2002); however, the northern extent of the rupture associated with the 1960 M_w = 8.1 foreshock is not clear (Cifuentes, 1989). Campos et al. (2002) assumed that this rupture propagated only southward because no land-level changes were reported north of ~37°30′S by Plafker and Savage (1970), including Isla Santa María. However, their survey was done eight years after the earthquake, and thus the M_w = 8.1 foreshock could have ruptured at least part of the Concepción segment releasing some of the accumulated strain and preventing the occurrence of an interplate earthquake since.

Coseismic uplift on Isla Santa María had been previously described, but not quantified for the M ~ 8.5 earthquake in 1751, which had a related tsunami that completely destroyed the city of Penco, causing the relocation of this former regional capital to its present-day position in Concepción (Lomnitz, 1970). The island is also located in the rupture zone of the 20 February 1835 earthquake, which had an estimated magnitude of 8.25 (Lomnitz, 1970). Coincidently, Charles Darwin and Captain Robert FitzRoy were in this area during the earthquake and visited the island twice, from 4–7 March and from 27 March–17 April (Darwin, 1839; FitzRoy, 1839; Darwin, 1851). During the first visit, they concluded from dead shellfish, water marks, soundings, and verbal testimony of the inhabitants that the land had been raised ~2.7 m; during their second visit, three precise measurements were made: 2.4, 2.7, and 3.0 m in the southern, central, and northern sectors of the island, respectively (Fig. 2B). These land-level changes were obtained using the emerged upper limit of dead *Mytilus* shells exposed at rocky cliffs as a pre-earthquake marker of the upper limit of the intertidal zone. They also measured uplift on the mainland of 1.8, 2.4, and 1.5 m at Tubul, Isla Quiriquina, and Talcahuano harbor, respectively (Fig. 2B). At the latter locality ~50% of postseismic recovery was observed during the two months following the earthquake. One month after the earthquake, Simón Rodríguez made a formal report of the damages, which also mentions 2.4–3.0 m of uplift at Isla Santa María (Rodríguez, 1835).

The abrasion platform that emerged during the 1835 earthquake is exposed as a prominent feature around the entire island (Fig. 4). Interestingly, the present-day elevation of the platform is similar to its position as measured by Darwin. The abrasion platform is tilted to the east with heights of 2.6–3.2 m above the high-tide level along the western coast, whereas it only reaches 1.6–2.0 m at the eastern coast.
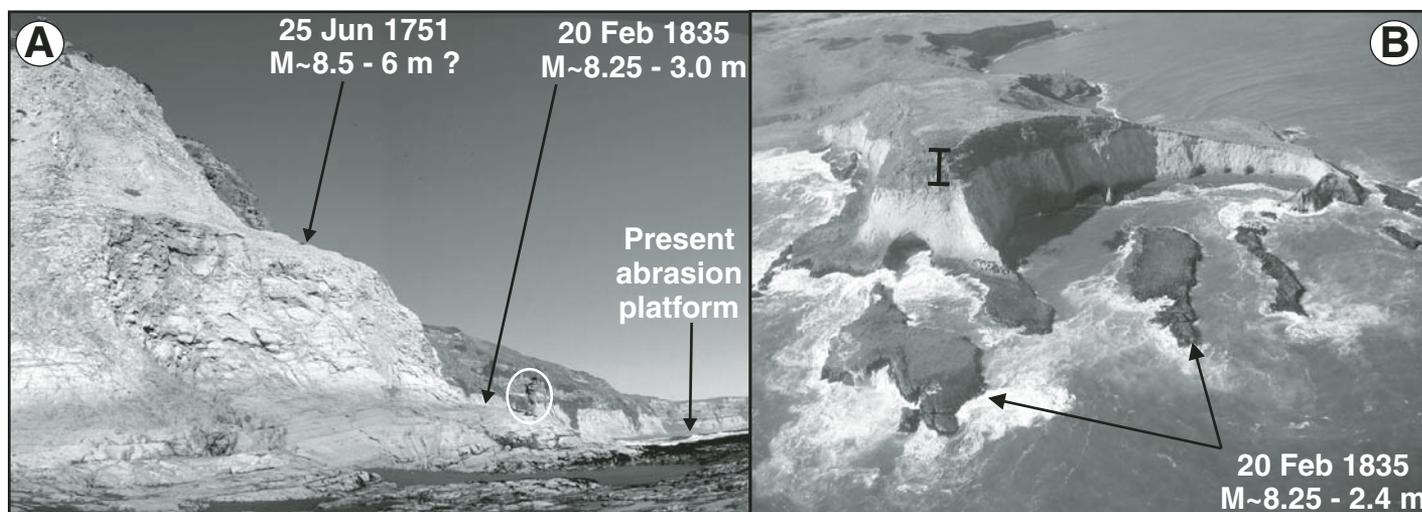
Figure 4. (A) View of the two preserved uplifted abrasion platforms on the northwestern coast. These surfaces were abandoned due to coseismic uplift, probably during the two last great earthquakes. The lower platform was abandoned by the 3.0 m of coseismic uplift during the 1835 M ~ 8.25 earthquake (Darwin, 1839; magnitude from Lomnitz, 1970). Uplift was also described, but not quantified, during the 1751 M ~ 8.5 earthquake (Lomnitz, 1970), which may have reached ~6 m. Person in white circle is for scale. (B) Aerial view of the abrasion platform emerged during the 1835 earthquake at the southern tip of the island. This surface reaches 2.6–3.2 m along the western and 1.6–2.0 m along the eastern coast, which is consistent with the amount of coseismic uplift documented by Darwin (1839), and is indicative of coseismic eastward tilting. The bar indicates the location of the Punta Cochinos section shown on Figure DR2 (see text footnote 1).

STRATIGRAPHY OF ISLA SANTA MARÍA

Isla Santa María is composed of two distinct sedimentary units: the Tertiary substrate formed by well-lithified sedimentary rocks, and Pleistocene marine and continental, poorly consolidated deposits that follow over a marked angular unconformity (Fig. 5). Our radiocarbon ages obtained from the base of the Pleistocene sequence (Table 1) constrain the onset of renewed marine sedimentation to a minimum age of 53 ka. We define and name this sequence the Santa María Formation.

Tertiary Sedimentary Rocks

The Tertiary sedimentary units include (Fig. 3A) the late Eocene Millongue Formation (Muñoz-Cristi, 1946) and the late Miocene to early Pliocene Ranquil Formation. These units are composed of sandstone and shale containing coal seams, and massive white siltstone and fine sandstone, respectively. The Millongue Formation is only locally exposed, whereas the Ranquil Formation crops out almost continuously along the cliffs, except at the center of the island (Fig. 3A).

Pleistocene Santa María Formation

The Santa María Formation can be differentiated into two distinct units: a lower, dominantly marine shore unit with interbedded nearshore terrestrial beds and an upper unit composed of eolian sands (Fig. 6).

Lower Marine Unit

The lower unit of the Santa María Formation is continuously exposed along the western coast, whereas in the east, it is discontinuous (Fig. 3A). The maximum thickness of 78 m is on the southwestern coast, where marine deposition occurred in topographic lows in the undulatory Tertiary substrate (Fig. 5). In our latitudinal transects, the thickness was found to always increase eastward (Table DR1).[1] These beds consist of predominately medium to coarse sandstone with interbedded layers of paleosol, peat, and clay. Descriptions of facies, grain-sizes, and sections are available in the GSA Data Repository (see footnote 1). We propose that this unit was deposited in a marine nearshore environment based on the occurrence of coarse landward-inclined crossbedding, wavy flaser bedding, intense vertical bioturbation, occasional occurrence of shell

---
[1]GSA Data Repository item 2006176, description of facies and trace fossils, sedimentology, grain-size curves, stratigraphic sections, and field photos of the Santa María Formation; description and field photos of facies filling incised channels; description and field photos of normal faults and related growth strata; tilt rate calculation procedure and tables with field data and average values, is available on the Web at http://www.geosociety.org/pubs/ft2006.htm. Requests may also be sent to editing@geosociety.org.

fragments, and similarities in grain-size distribution with present-day deposits.

We obtained four radiocarbon ages from paleosol, peat, and clay layers at the base of this unit (Fig. 3A; Table 1). The sample at the southeastern coast yielded a lower bound of 42 ka, and north of the Cadenas Peninsula, a lower bound of 53 ka; in the southwestern sector, we obtained ages of 52.7 ± 2.5 ka and 48.8 ± 1.3 cal ka (cal ka = calibrated thousand yr B.P.). From similar layers interbedded in the marine sands, we obtained five ages, which range between 45.3 ± 1.7 and 48.4 ± 2.1 cal ka (Table 1). The samples constitute centimeter-size wood fragments devoid of any sign of contamination by younger roots.

Upper Eolian Unit

In map view, most of the Santa María Formation consists of very well sorted, semi-consolidated gray to brownish sandstone. We distinguish this succession as the upper stratigraphic unit of the Santa María Formation. The contact with the underlying marine-dominated unit is conformable and transitional. The thickness reaches a maximum of 14 m at the western, and 37 m at the eastern coast, increasing northeastward in the southern domain, and southeastward in the northern domain. It thus mimics the depositional pattern of the underlying marine unit. This unit comprises a characteristic rhythmic succession of homogeneous beds with alternating horizontal and inclined parallel lamination
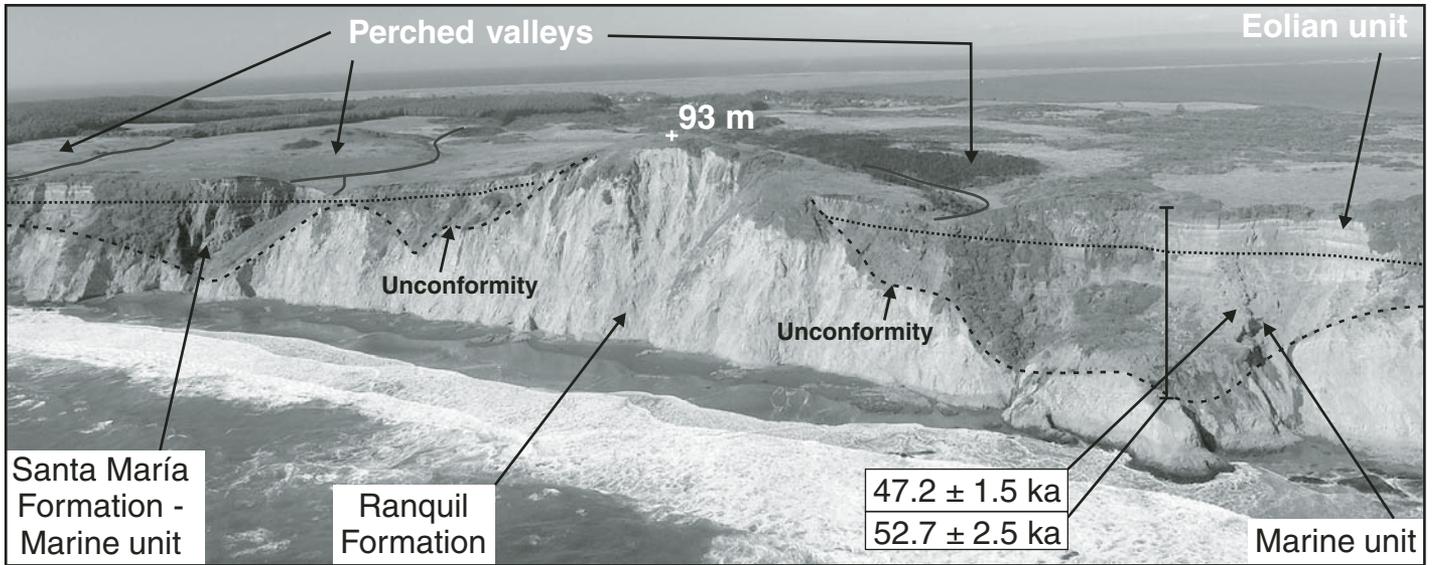
Figure 5. Oblique aerial view to the east in the south of the island; see Figure 3B for location. Note the marked unconformity between the Tertiary siltstone and the late Pleistocene Santa María Formation, and the color contrast between the marine and eolian units. The perched morphology of the valleys is interpreted as having been produced by progressive cliff retreat. The bar indicates the location of the Trampa del Diablo section shown on Figure DR2 (see text footnote 1).
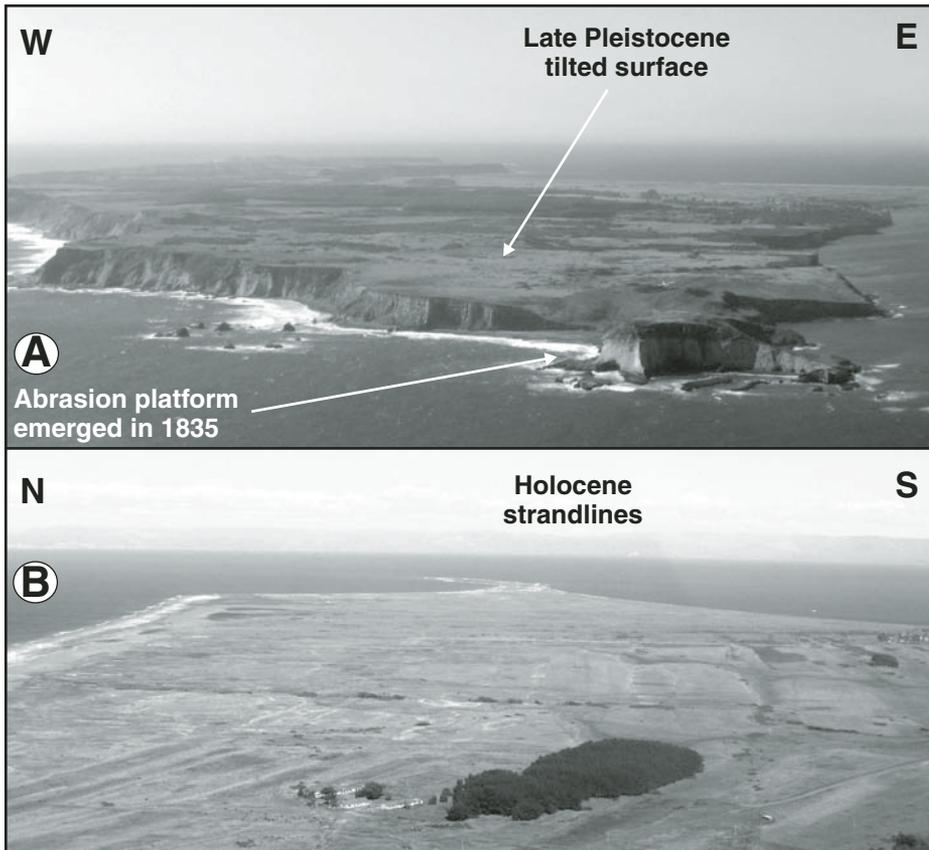

Figure 6. (A) Oblique aerial view to the north of Isla Santa María. Note the eastward tilt of the upper surface and the lowlands on the eastern part. The abrasion platform abandoned after the 1835 earthquake can be seen. (B) Oblique aerial view to the east of the Holocene lowlands with emerged strandlines forming the undulatory landscape.

(Figs. 6 and 7). Descriptions of facies, trace fossils, and sedimentary sections are available in the GSA Data Repository (see footnote 1). The beds with inclined laminations uniformly dip 20–30° throughout the island, and the dip direction is parallel to the northeast direction of the prevailing Pacific winds. Grain-size distributions from this unit and from active dunes of the island are very similar and contrast markedly with the underlying unit (Fig. DR1, see footnote 1). We interpret a continental, eolian depositional environment for the upper unit of the Santa María Formation. A paleosol at the base of this sequence yields a radiocarbon age of 31.5 ± 1.8 cal ka (Table 1; Fig. 3A; Fig. DR8 [see footnote 1]).

Compared to recent depositional environments, eolian sand dunes in low-relief coastal regions and islands are active only when they are at elevations below ~15–20 m, as seen in the present-day distribution of coastal eolian environments in south-central Chile (Paskoff and Manríquez, 2004) and a detailed correlation between late Quaternary sea-level highstands and eolian activity (Carr et al., 2006). The sea-level curve of Siddall et al. (2003) shows that between the onset of eolian activity at 31.5 ka and 27.5 ka, sea level was fairly stable at −82.2 ± 6.1 m. At 27.5 ka, sea level started to fall continuously to reach its lowermost level of −114 m during the Last Glacial Maximum (LGM) at 19.5 ka. Thus, based on the onset of eolian deposition at 31.5 ka, we infer that the dune
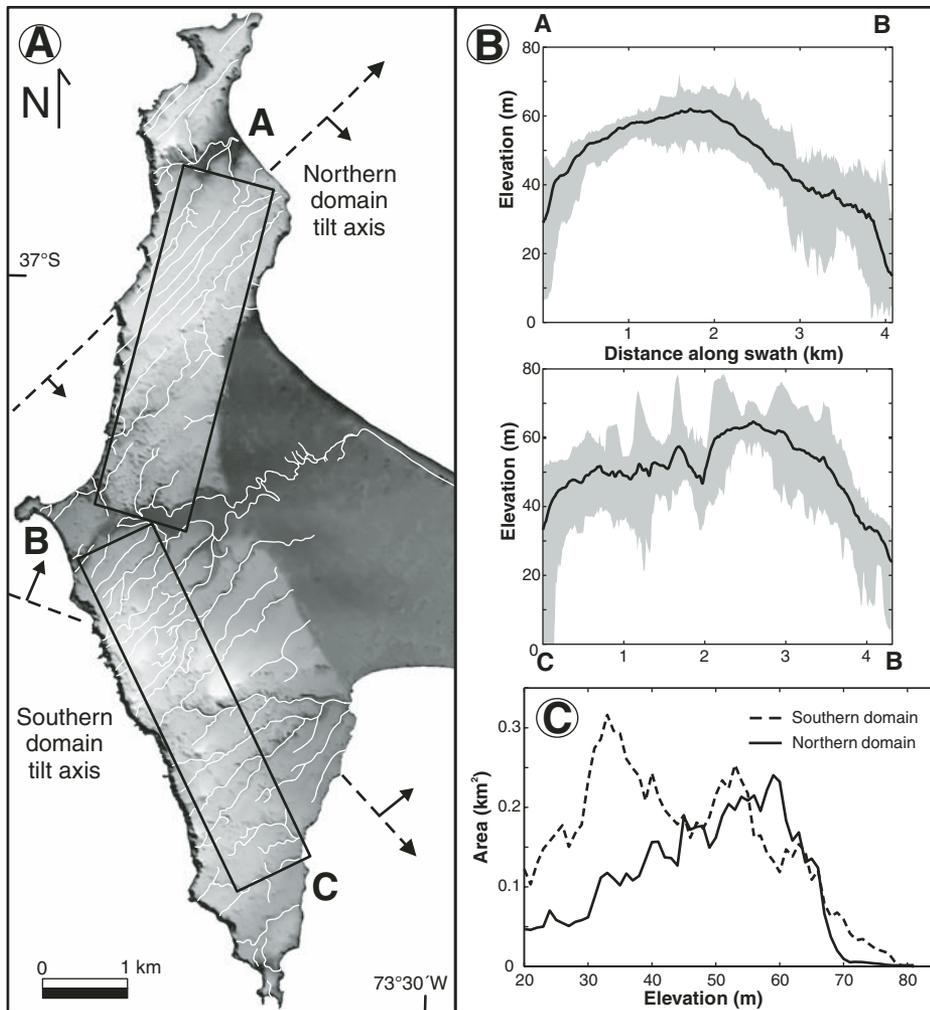
Figure 7. Topographic asymmetry of the upper surface of Isla Santa María. (A) Digital elevation model (DEM) with drainage network. Note the asymmetric tilt of the upper surface. (B) Swath topographic profiles from areas shown on the DEM. The thick line represents the mean topography, and the shaded area, the maximum and minimum values, respectively. (C) Hypsometric curves derived from the DEM for the entire northern and southern domains of the upper surface. The DEM was split along the central valley to derive these curves. Note the differences in morphology and distribution of topography in both domains.

fields were deposited between 31.5 ± 1.8 and 27 ± 2 ka.

Fluvial System and Channelized Holocene Debris-Flow Deposits

The eolian unit of the Santa María Formation is incised by linear ephemeral channels (fluvial system in Fig. 3A). In the southern domain, the drainage channels follow the slope of the upper surface due to the tilt of the island about a west-northwest axis. In contrast, in the northern domain, the drainages have a marked parallel pattern, which is influenced by the orientation of recent faults and fractures (Fig. 3). The channels

are carved into the Santa María Formation, and near the Cadenas Peninsula, they are filled by debris-flow deposits (Fig. 3A). These deposits are massive, monomict and are composed of brownish sandstone clasts from the eolian unit of the Santa María Formation (Fig. DR5, see footnote 1); the matrix constitutes brown sand and peat containing wood. In the southern channels, at least three superimposed debris-flow deposits occur; the upper two provided radiocarbon ages of 7.66 ± 0.03 and 6.70 ± 0.02 cal ka (Figs 3A). In the northern part of the peninsula, we obtained ages of 8.90 ± 0.09 and 7.73 ± 0.04 cal ka from similar deposits (Table 1). These debris-flow deposits, however, cannot be used to

calculate uplift rates because their position with respect to paleo–sea level is ambiguous, because of cliff retreat and eastward tilting. In addition, the southern deposits occur in the hanging wall of normal faults (Fig. DR7, see footnote 1).

The age of these deposits indicates that by ca. 9 ka, processes leading to the semiconsolidated eolianites of the Santa María Formation had been long inactive. Incision and development of the drainage network must thus have started between ca. 27 and 9 ka, and was probably related to sea-level fall during the LGM at ca. 19.5 ka.

GEOMORPHOLOGY OF ISLA SANTA MARÍA

In map view, Isla Santa María has an east-pointing triangular shape (Fig. 3A). We subdivided the island in two main geomorphic units: (1) a central part formed by a higher surface tilted <2° landward and bounded by steep cliffs (Figs. 3 and 6A), here denoted as the upper surface; and (2) lowlands east of the upper surface, which form an east-pointing wedge and comprise a sequence of emerged strandlines, marshes, and dunes (Figs. 3 and 6B). The upper surface is formed by poorly consolidated sediments of the Santa María Formation (Fig. 5).

Upper Surface

The upper surface consists of a northern and southern domain, divided by an east-west–oriented central valley, which integrates the main drainage of the island (Fig. 3). We derived a hypsometric curve for each domain, which shows the asymmetric distribution of topography (Fig. 7B). The eastward tilt of the upper surface is also asymmetric and has different tilt axes, as also seen on topographic swath profiles (Fig. 7C) and the thickness distribution of the Santa María Formation (Table DR1, see footnote 1). The southern domain is tilted to the north-northeast, along a west-northwest–striking axis, while the northern domain is tilted to the southeast, along a northeast-striking axis.

Lowlands—Holocene Emergent Strandlines

The emerged strandlines, marshes, and dunes in the lowlands occur at elevations up to 18 m (Fig. 6B). The southern part of these lowlands is exposed to the strong southwesterly Pacific winds and thus governed by northeast-oriented blowouts and dunes. However, the northern part is in the lee of the upper surface, allowing the preservation of emerged strandlines (Fig. 3). Twenty strandlines are well preserved, and approximately five more are covered by dunes.
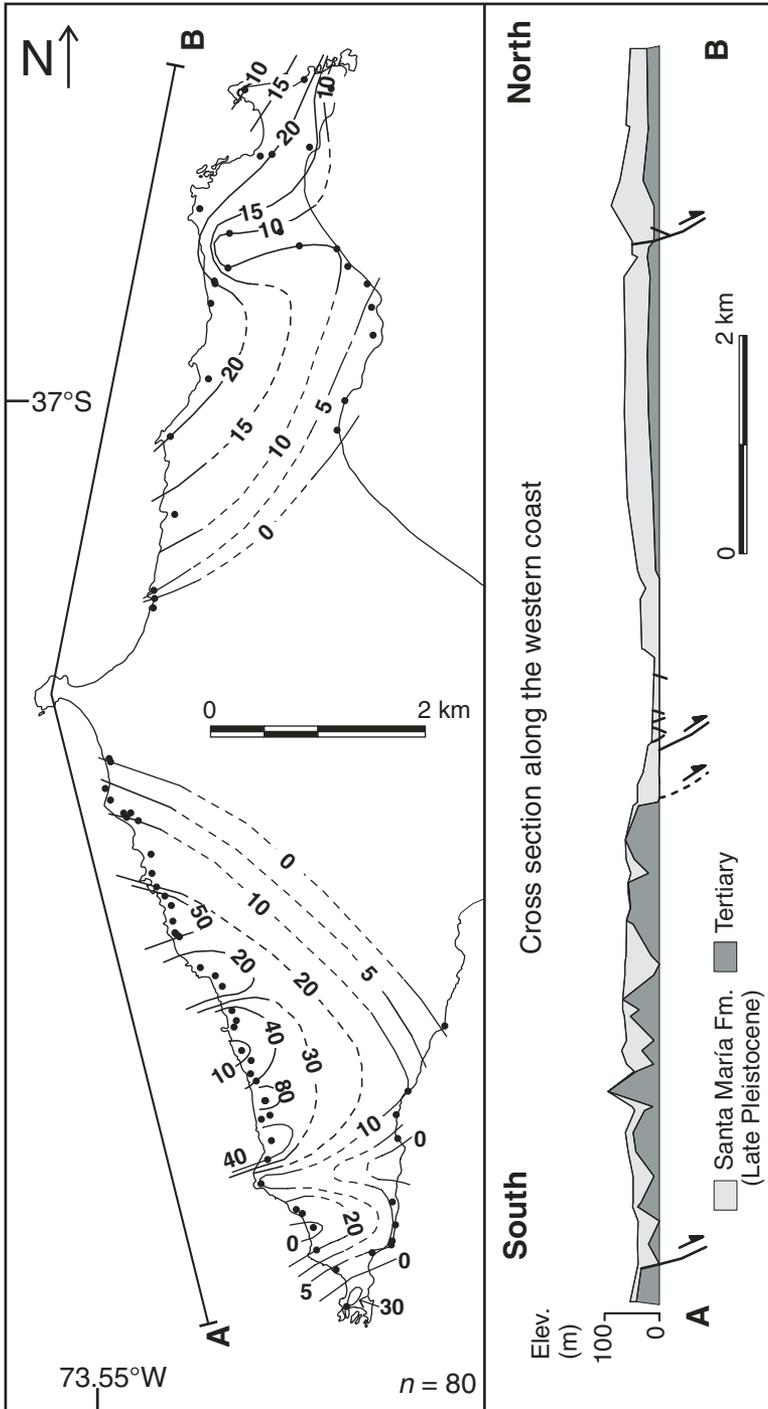
Figure 8. Contour map of the base of the Santa María Formation and N-S profile along the western coast of the island. Note the marked asymmetry of the island in both map view and cross section. The southern domain is tilted to the NNE along a WNW-striking axis, while the northern domain is tilted to the WSW along a NNE-striking axis. Black dots on the map correspond to data points measured at sea cliffs with a digital altimeter and tape. Note the similarity between the surface of the island (see digital elevation model in Figs. 3B and 7) and the Tertiary–Pleistocene unconformity surface.

The strandline sequence is formed by parallel pairs of beach berms and back-swamps that result in an undulating, shore-parallel landscape of ridges and depressions (Fig. 6B). The berms consist of medium well-sorted black sand, while the back-swamp areas consist of organic-rich, homogeneous silty sand. The crests reach 12 m elevation and are late Holocene in age, as shown by eight 3.4 to 1.8 ka luminescence ages obtained from the central part of the sequence (Bookhagen et al., 2005, 2006).

The formation of such a landscape in a shore-line environment is only plausible with a rather stable sea level affected by successive episodes of relative sea-level fall, caused by tectonic uplift and/or postglacial isostatic rebound (e.g., Matsuda et al., 1978; Nelson and Manley, 1992; Berryman, 1993a; Ota and Yamaguchi, 2004; Stewart et al., 2000). At Isla Santa María, post-glacial rebound can be rejected, because at this latitude, Pleistocene glaciers were restricted to the Main Cordillera at elevations above ~2000 m (Rabassa and Clapperton, 1990), ~180 km east of the island (Fig. 1A). Thus, tectonic uplift by either repeated coseismic events and/or pro-tracted aseismic movements must have caused the emergence of these strandlines.

PALEOGEOGRAPHY OF THE SANTA MARÍA FORMATION

Identical depositional environments with which we correlate the late Pleistocene Santa María Formation exist on the island today: beaches with black sands surround the island; swamps occur in the lowlands and central valley; and dune fields cover the lowlands (Fig. 3A). We interpret that the cyclic interbedding of black marine sandstone and clay-rich continental layers, and the graded sandstone represent a mixed signal of tectonic uplift and eustatic sea-level oscillations. The fact that the upper unit of the Santa María Formation is exclusively eolian, and that its base is ca. 31 ka in age, when sea level must have been ~90 m lower than at present, emphasizes that tectonic uplift during the late Pleistocene has outpaced glacio-eustatic oscillations in this environment.

TOPOGRAPHY OF THE TERTIARY-PLEISTOCENE UNCONFORMITY AND MARINE-EOLIAN TRANSITION SURFACES

Exposures of the unconformity between the Tertiary and Pleistocene units are ubiquitous along the western and northeastern coasts of the island and show a pronounced variation in elevations (Figs. 5 and 8). The geometry of the unconformity has a marked north-south

asymmetry, segmented by the central valley, where the unconformity is below sea level. The north-south profile shown on Figure 8 was constructed with measurements obtained at the western coast. This profile illustrates the longitudinal asymmetry of the island and the pronounced paleorelief in the southern part. There, the unconformity is very undulatory, reaching over 80 m elevation in the highest hills of the island (Figs. 5 and 8). The strong paleorelief in the south contrasts with the north, where the unconformity is subhorizontal and lies at elevations between 10 and 20 m.

The contour map of the Tertiary–Pleistocene unconformity also exhibits a contrasting geometry between the south and north of the island (Fig. 8). The surface is inclined, northeast-striking, and southeast-dipping in the northern part, whereas in the south, it strikes northwest and dips northeast. Interestingly, the asymmetric tilt of the unconformity is very similar, but steeper, when compared to the inclination and geometry of the present-day surface of the island (Fig. 7A). We interpret the strong paleorelief of the unconformity in the south of the island to result from fluvial erosion of the continental shelf region during early Pleistocene sea-level lowstands. The bathymetric map (Pineda, 1999) has similar undulatory contour lines southwest of the island (Fig. 2D), and multibeam bathymetry (Reichert et al., 2002) reveals a submarine canyon immediately west of the island (Figs. 1B and 2A), related to former fluvial systems. Subsequently, the former channels were filled with marine nearshore deposits of the Santa María Formation.

The conformable transition between the marine and eolian units in the Santa María Formation also has a similar geometry as the Tertiary–Pleistocene unconformity, involving a general decrease in elevation eastward along the entire island, and the same asymmetric geometry in map view. These observations indicate that Pleistocene marine and eolian deposition was synchronous with progressive asymmetric tilting. Hence, uplift and tilting of the island during the Pleistocene must have been governed by identical processes as those responsible for the present-day tilting of the island (Figs. 6A and 7A).

NORMAL FAULTING AND SYNTECTONIC SEDIMENTATION

In contrast to the pervasively faulted and fractured Tertiary rocks, the Santa María Formation is cut by faults only in three areas. All Quaternary faults are extensional, steeply dipping, and strike northeast to east-northeast. They are located at the north, center, and south of the island, ~5 km from each other (Figs. 3A and 8). Adjacent to

the faults, liquefaction features and growth strata are ubiquitous in the marine unit of the Santa María Formation. Well-preserved ruptures indicate very recent activity along the northern and central faults. Detail descriptions and photos are in the GSA Data Repository (Figs. DR6–DR8). The constant dip of individual growth strata is indicative of domino-style block rotation controlled by high-angle normal faults.

LATE QUATERNARY DEFORMATION RATES OF ISLA SANTA MARÍA

Uplift Rates

We calculated uplift rates from dated paleosols, peat, and clay layers from the Santa María Formation. We interpret these beds as geomorphic markers of back-swamp areas in the immediate vicinity of corresponding paleo–sea level positions, since, at present, identical depositional environments and facies associations are exclusively found near sea level or at elevations that are within the error of the sea-level curve (±12 m). Table 1 presents ten AMS radiocarbon ages from these layers. In order to derive realistic uplift values and uplift rates, we viewed the sample elevations with respect to the position of their present counterparts and the late Pleistocene sea-level curve of Siddall et al. (2003). The resulting ages from the marine unit correspond to uplift rates between 1.2 ± 0.35 and 2.3 ± 0.36 m/k.y., but the age of a single sample from the base of the fixed dunes at the southern point of the island provided a significantly higher rate of 4.0 ± 0.28 m/k.y. (Fig. 9; Table 1).

We attribute the twofold difference in uplift rate between the sample at the southern point of the island and the rest of the samples from the marine unit to be related to normal faulting rather than an acceleration of uplift. Since the marine unit is absent at the southern tip of the island, footwall uplift caused by normal faulting may be responsible for its absence and the higher degree of uplift there (Fig. DR8, see footnote 1). Samples collected in the central depression are in the downthrown blocks of normal faults and, hence, have lower uplift rates. Averaging all the ages yields an uplift rate of 2.01 ± 0.38 m/k.y.; however, by removing the footwall sample, we obtain a more realistic rate of 1.79 ± 0.39 m/k.y. Because the radiocarbon ages are on the analytical limit of the dating method, this uplift rate should be considered a maximum value.
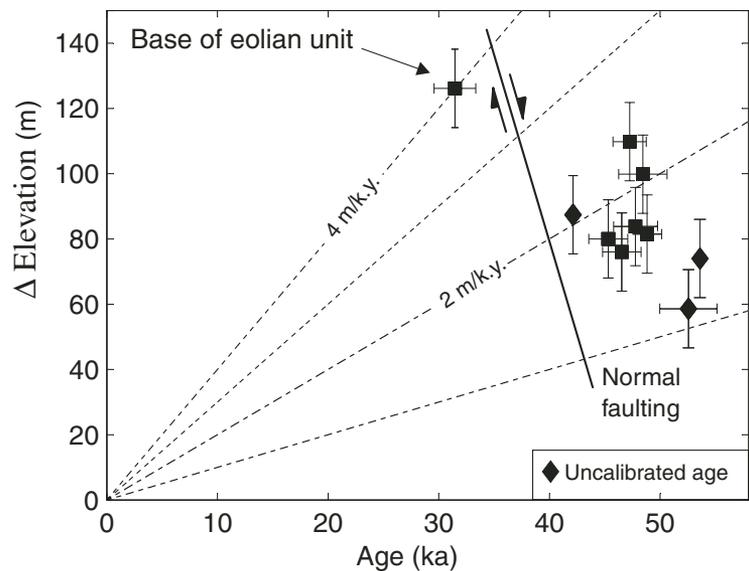

Figure 9. Uplift rates of Isla Santa María. Squares are calibrated accelerator mass spectrometry (AMS) ^{14}C ages with 2σ error bars. The samples are from paleosol, peat, and clay layers from the nearshore marine unit, and one from the paleosol at the base of the eolian unit of the Santa María Formation. We assumed that they originated near sea level because, at present, the same depositional environments occur only near sea level at the island. Δ Elevation is equal to the present altitude of the samples minus the paleo–sea-level elevation from the Siddall et al. (2003) data set, which has a 12 m 2σ error. We attribute the difference between the 4.0 ± 0.28 m/k.y. uplift rate calculated for the sample at the base of the fixed dunes and the rest of the samples to the effects of normal faulting. The mean uplift rate is 2.0 ± 0.38 m/k.y., and by removing the footwall sample, 1.79 ± 0.39 m/k.y.

Interestingly, despite this uncertainty, the late Pleistocene uplift rate agrees within error with the late Holocene uplift rate of 2.1 ± 0.1 m/k.y. derived from the strandline sequence (Bookhagen et al., 2006).

Tilt Rates

We used three reference surfaces to calculate late Pleistocene tilt rates of the island: (1) the ca. 50 ka Tertiary–Pleistocene unconformity and base of the marine unit; (2) the horizon of the marine-eolian transition, which marks the emergence of the island and onset of subaerial deposition at 31.5 ± 1.8 ka; and (3) the present surface of the island, which is depositional and has an age of 27 ± 2 ka. From our field observations, we infer that these erosional/depositional surfaces were subhorizontal at the time of their abandonment. The elevation of each of these surfaces was correlated across eight detailed sections normal to the tilt axes of each domain (Fig. DR9 and Table DR1, see footnote 1). We obtained average tilt rates of 0.024 ± 0.014°/k.y. for the Tertiary–Pleistocene unconformity, 0.039 ± 0.022°/k.y. for the base of the eolian unit, and 0.031 ± 0.016°/k.y. for the present surface of the island. Averaging all these values yields an integrated tilt rate for the island of 0.032 ± 0.018°/k.y. during the past ~50 k.y. (Table DR2, see footnote 1).

The average late Holocene tilt rate calculated from a detailed topographic survey of the emergent strandlines and luminescence ages is 0.020 ± 0.001°/k.y. (Bookhagen et al., 2006), which suggests rather steady tilting during the late Quaternary.

ACTIVE SHORTENING AND BASIN INVERSION STRUCTURES

Our observations clearly show that Isla Santa María has been uplifting and tilting in two asymmetric tilt domains at a relatively constant rate during the late Quaternary. In order to explain and decipher the mechanisms responsible for this deformation, we first view our interpretations in the framework of offshore seismic-reflection profiles, local network seismicity data, and focal mechanism solutions. In a second step, we integrate these geophysical data with the geologic and geomorphic observations to propose that active crustal reverse faults are responsible for the differential surface deformation on the island and in the neighboring Arauco-Concepción area.

Crustal Seismicity

Data from the temporary ISSA local network show that most of the seismicity within the upper plate is concentrated in the forearc below the coast and shelf. Sixty-one crustal events cluster 7 km north of Isla Santa María in an area of ~90 km^2 (Fig. 2D). In an east-west section, seismicity has a linear alignment inclined 67°W that extends from 0.6 km depth to the plate interface at ~12 km; below this depth, seismicity becomes scattered (Fig. 1C). Bruhn (2003) calculated focal mechanism solutions for two M_w = 4.0 events, which are both very similar and compatible with a 022°E-striking, 72°W-dipping reverse fault with a minor dextral strike-slip component (Fig. 2C). The fact that the dip of the two focal mechanisms is very similar to the inclination of the earthquake alignment suggests that this concentration of seismicity underneath Isla Santa María is caused by a crustal-scale reverse fault. On 21 May 1990, a 5-km-depth, M_w = 6.2 earthquake reported in the U.S. Geological Survey National Earthquake Information Center (USGS-NEIC) catalogue occurred east of the island, also with a focal mechanism compatible with a north-northeast–striking steep reverse fault (Fig. 2D). Recent data from another local network confirm the cluster of shallow seismic activity northeast of the island (Rietbrock et al., 2005).

Shortening Features Imaged from Seismic-Reflection Profiles

We interpreted offshore seismic-reflection profiles covering an area of ~1800 km^2 surrounding Isla Santa María (Fig. 2C). The base of the late Pliocene to Pleistocene Tubul Formation has been correlated with a high-amplitude reflector recognized in all profiles that truncates older sequences, and in four ENAP hydrocarbon exploration boreholes located southeast of the island (Fig. 2C) (Mordojovich, 1981; González, 1989; Elgueta and Arcos, 1994; Vietyes et al., 1993). The base of the Tubul Formation is a key horizon that brackets the minimum age for the onset of basin inversion and syncontractional sedimentation at 2.5 Ma. The maximum age for inversion of 3.6 Ma is provided by foraminifera and ostracodes from the underlying synextensional Ranquil Formation.

East-Vergent Faults and Folds Northeast of Isla Santa María

Reflection profile 017 is oriented west-northwest and situated 6 km north of the island crossing the cluster of crustal seismicity (Figs. 2C and 2D). This profile reveals three shortening structures (Fig. 10): (1) an asymmetric anticline at shotpoint (SP) 500; (2) an east-dipping monocline at SP 250; and (3) an east-vergent ramp at SP 150. The crest of the anticline is obscured by horizontal seafloor multiples at ~0.4 and ~0.3 s depth (two-way traveltime). Several small discontinuous reflectors are offset below the anticline, which we relate to a west-dipping reverse fault responsible for propagating this fold. Below the monocline, a reverse fault with an east-dipping asymmetric anticline in the hanging wall is clearly seen.

We identified a lower sequence, characterized by the lack of well-defined internal onlaps and truncations, and folding of subparallel, discontinuous reflectors. This unit consists of the Lebu Group and Ranquil Formation. The unconformably overlying upper unit corresponds to the Tubul Formation and exhibits onlaps, truncations, variations in thickness, progressive upward decrease in dip, and pinch-out of reflectors, which are indicative of syncontractional deposition. Two minor normal faults cut the strong uppermost reflectors above the anticline, which we interpret as crestal-bending faults. The axial surfaces of the monocline define an upward-narrowing zone above 0.4 s. Active growth here can be inferred because the apex of this growth triangle is at the present surface, which is depositional (Suppe et al., 1992). Line-length balancing of the 2.5-m.y.-old base of the syntectonic Tubul Formation accounts for 8% of shortening, and thus a minimum late Pliocene to Holocene shortening rate of ~0.8 mm/yr. The spatial coincidence of these structures with the inclined plane of crustal seismicity suggests that they are genetically linked with a ramp-flat-ramp geometry rooted in the plate-boundary thrust at ~12 km depth (Fig. 1C).

North-Vergent Faults and Folds East of Isla Santa María

Reflection profiles east of the island (Fig. 2C) reveal complex lower sequences corresponding to the Quiriquina Formation, Lebu Group, and Ranquil Formation (Vietyes et al., 1993), which are affected by normal faults (Figs. 11 and 12). Some of these faults are inverted and control the occurrence of folds deforming the unconformably overlying Tubul Formation. These inverted faults are recognized in all profiles of the southeastern Arauco Bay (Fig. 2C), from which we deduced a west-northwest strike.

Profile 016 images five south-dipping normal faults between shotpoints 400 and 800 and one north-dipping normal fault to the north of SP 400 (Fig. 11). These structures controlled tilting of domino-style blocks and synextensional deposition of the Lebu Group and Ranquil Formation. Two faults cut the Tubul Formation and determine the occurrence of fault-related folds. Onlaps within the Tubul Formation occur on the limbs of these fault-related folds, indicating syncontractional deposition. The reverse faults at the core of these anticlines have normal offsets
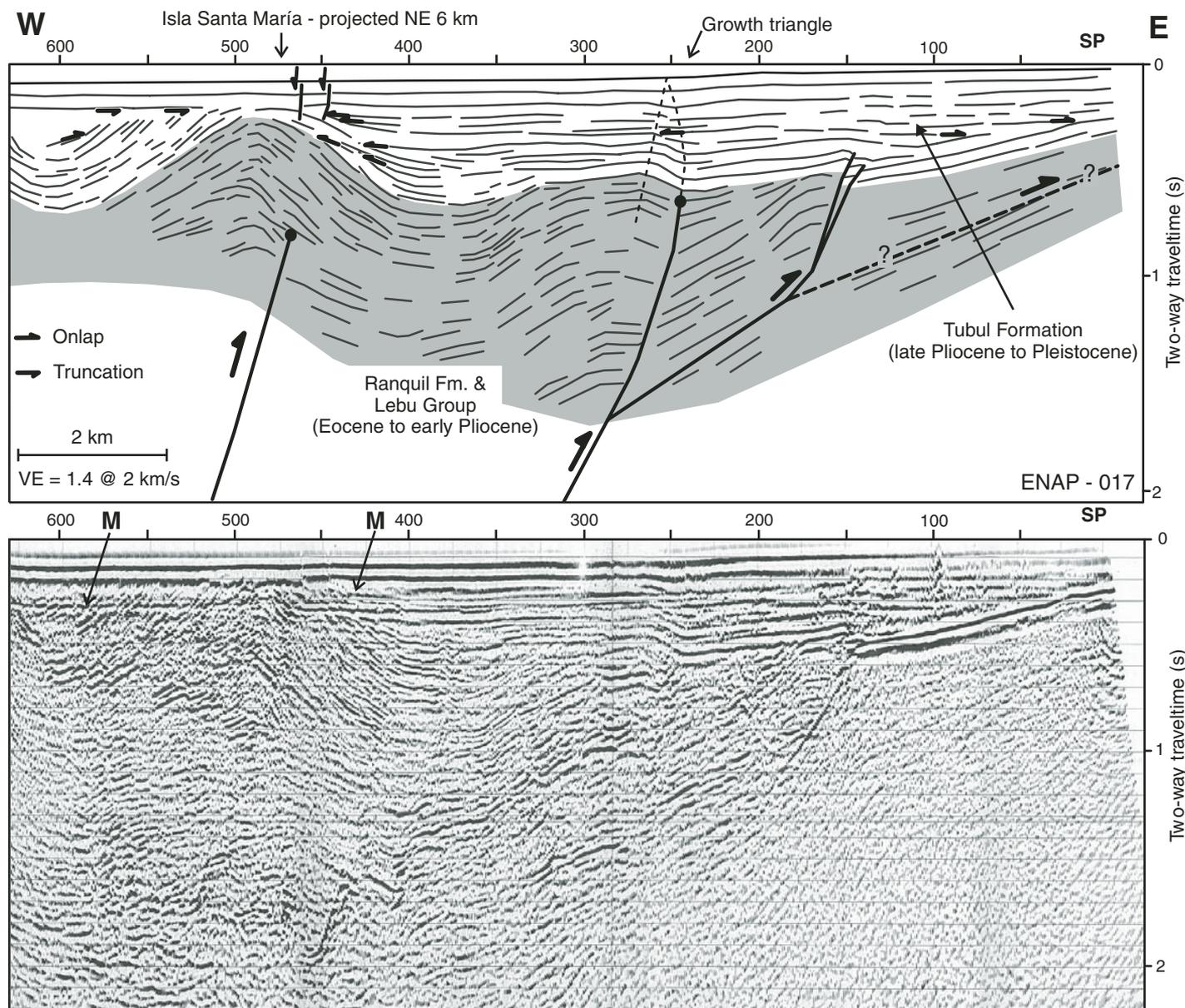
Figure 10. Migrated seismic-reflection profile ENAP-017 (24-channel). See Figure 2C for location. The syntectonic sequence shows eastward propagation of the deformation by footwall shortcuts. The fault below the anticline is inferred to be rooted in the plate interface area at ~12 km depth, which is supported by the continuous alignment of seismicity (see Fig. 1C). M—seafloor multiple.

in the lower units, and thus are likely inverted normal faults of the Late Cretaceous to early Pliocene extensional Arauco Basin. The anticline at SP 630 has a west-northwest–striking axis, which passes nearly through the easternmost point of the island and the southern shore of the lowlands; it appears to be an active structure deforming the uppermost reflectors (Fig. 11). Profiles 259 (Fig. 12) and 257 (Fig. 13) image similar normal faults that controlled dominostyle block tilting and synextensional deposition of the Lebu Group and the Ranquil Formation in half-grabens. Folding of the unconformably overlying Tubul Formation and internal onlaps are observed in the vicinity of inverted normal faults. Profiles 016, 259, and 257 (Fig. 2C) show that structural relief across the north-vergent fault increases toward the island.

DISCUSSION

Uplift and Deformation Mechanisms of Isla Santa María

We have shown that the topography of the Tertiary–Pleistocene unconformity, marine-eolian transition surface of the Santa María Formation, and the present-day surface of the island are asymmetrically tilted in two separate domains. In the southern domain, these reference surfaces are progressively tilted to the north-northeast along a west-northwest–striking axis, while in the northern domain, they are gradually tilted to the southeast along a northeast-striking axis (Figs. 7 and 8; Table DR1 [see footnote 1]). Furthermore, our analysis of seismic profiles revealed two systems of fault-cored anticlines in the Arauco Bay area: a northeast-striking system located northeast of the island and a west-northwest–striking one to
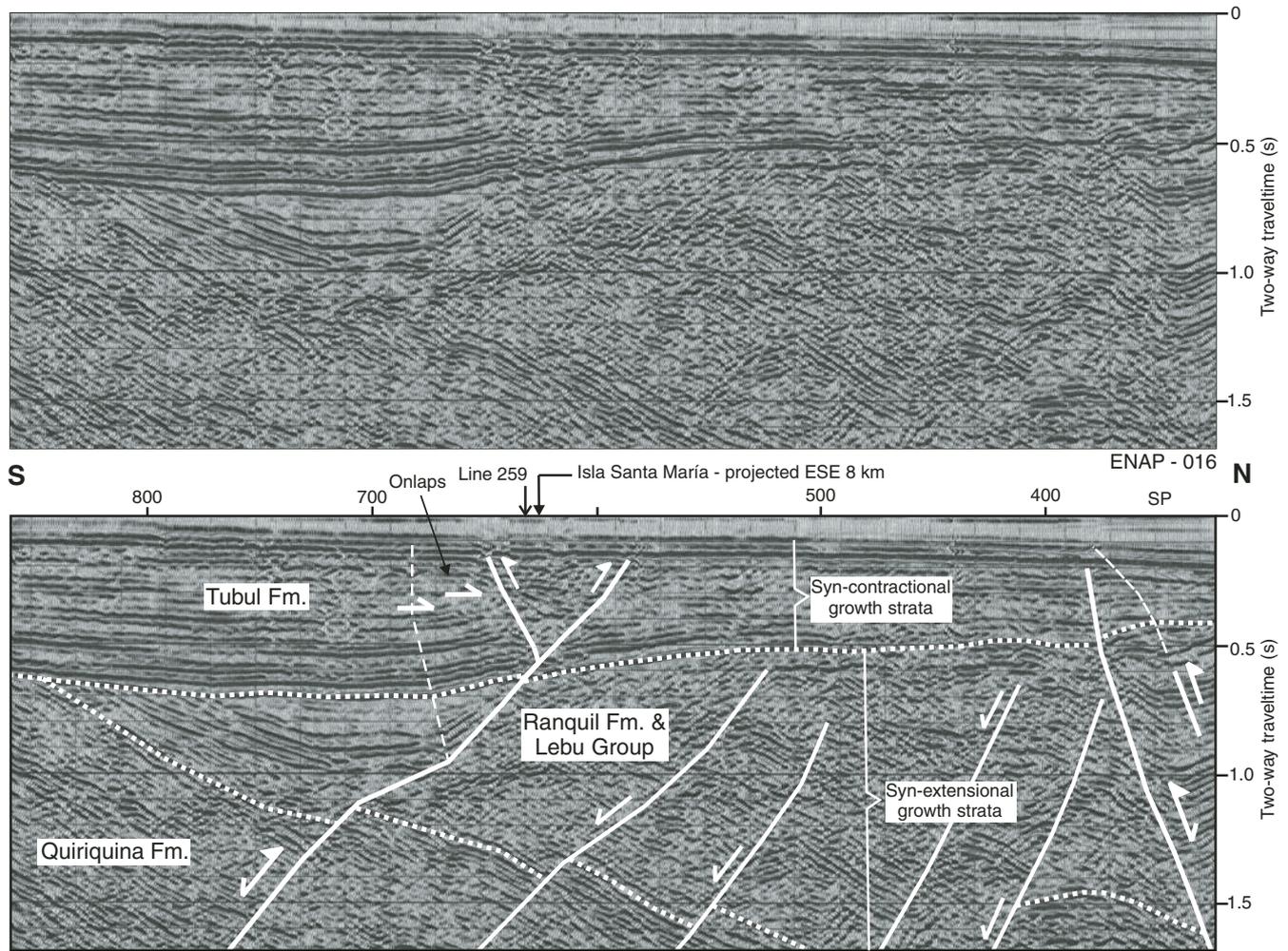
Figure 11. Migrated seismic-reflection profile ENAP-016 (48-channel). See Figure 2C for location. Stratigraphy is correlated with nearby exploration boreholes.

the southeast (Fig. 2C). Both systems converge at the center of the island and control the tilt asymmetry. Increased structural relief island-ward indicates lateral growth of the anticlines. The observed structural and geomorphic features of the island can thus be attributed to the convergence of two laterally propagating fault-cored anticlines. The eastward-tilted surfaces represent growth strata in the forelimbs of both folds, whereas their backlimbs have been removed by cliff retreat along the western coast of the island, which is exposed to strong wave attack by the Pacific Ocean (Fig. 14). Seismic-reflection profiles and exploratory well data reveal that the reverse faults in the core of the anticlines are inverted normal faults of the Late Cretaceous to early Pliocene extensional Arauco Basin, which explains their oblique orientation with respect to the margin.

The high-angle normal faults on the island are interpreted to be caused by tensile bending stresses in the crestal areas of these anticlines.

The marine growth strata adjacent to these faults corroborate extension as an integral part of folding, at least over the last ~50 k.y. The 10–15° angle between the axes of the anticlines and the strike of the crestal faults possibly reflect a small component of oblique shear (e.g., Philip and Meghraoui, 1983). This would result in oblique shortening with a small right-lateral component along the northeast-striking fold-fault system north of the island, which is corroborated by focal mechanisms (Fig. 2D).

Crustal Reverse Faulting, Coastal Geomorphology, and Megathrust Earthquakes

Based on our interpretation of seismic lines, we infer that the northeast-striking system of reverse faults and folds in the Arauco Bay extends from Isla Santa María to the Concepción area, where it apparently controls the morphology of the Hualpén, Tumbes, and Coliumo pen-

insulas, as well as Quiriquina Island (Fig. 2A). These are also topographic features related to anticlines that form a northeast-oriented en echelon arrangement. We therefore propose that in the Arauco-Concepción area, active upper-crustal reverse faults are responsible for creating topography. Furthermore, their orientation and distribution fundamentally control the coastal geomorphology reflected in elongated and aligned peninsulas, islands, and embayments. The reverse faults result from inversion of former Tertiary normal faults, the orientations of which were controlled by Paleozoic basement fabrics (González, 1989); this emphasizes the importance of inherited structures in guiding deformation in tectonically active regions. Inverted faults at Isla Santa María are analogous to inverted faults rooted in the Hikurangi subduction zone (Barnes et al., 2002).

The highest coseismic uplift recorded during the 1835 earthquake occurred along the fault-controlled islands and peninsulas of the
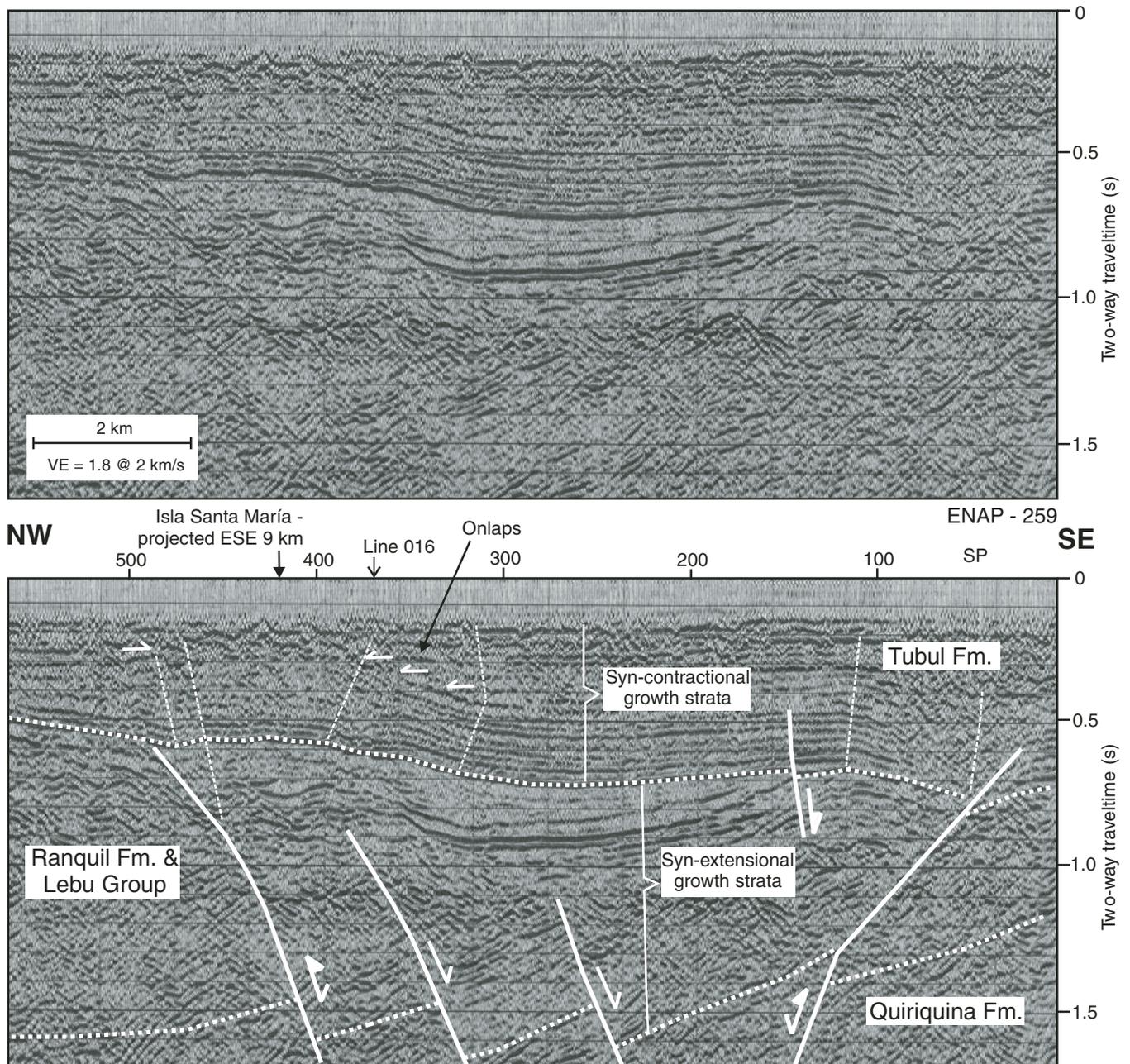
Figure 12. Migrated seismic-reflection profile ENAP-259 (48-channel). See Figure 2C for location. Stratigraphy is correlated with nearby exploration boreholes.

Arauco-Concepción area (Fig. 2B). Interestingly, the 2 m uplift contour related to this event is oriented northeast, and it is parallel to the elongation of these topographic features, as well as the reverse fault system (Fig. 2B). This spatial coincidence of geomorphic phenomena and inverted structures, as well as the fact that the uplifted abrasion platform at Isla Santa María is steeply tilted to the east, suggests that interplate mega-earthquakes may trigger slip on reverse faults in the upper plate. Consequently,

these structures would in turn control and localize the distribution of surface deformation. This assessment is supported by observations made during the 1964, M 9.2 Alaskan earthquake, which caused a maximum coseismic uplift of 11.3 m adjacent to the Patton and Hanning Bays reverse faults. Both structures were triggered by this event, causing at least 7.9 and 6.0 m of surface displacement, respectively (Plafker, 1972). Similarly, crustal-scale transverse faults along the Cascadia margin propagate surface folds,

which apparently control localized coseismic subsidence during megathrust ruptures (Goldfinger et al., 1992).

Coseismic warping and tilting caused by earthquakes nucleated in the low-angle megathrust are predicted by dislocation models (e.g., Savage, 1983) and are widely observed in geodetic data (e.g., Hyndman and Wang, 1995). The deformation patterns, and consequently the landforms associated with cumulative ruptures have wavelengths on the order of 100 km.
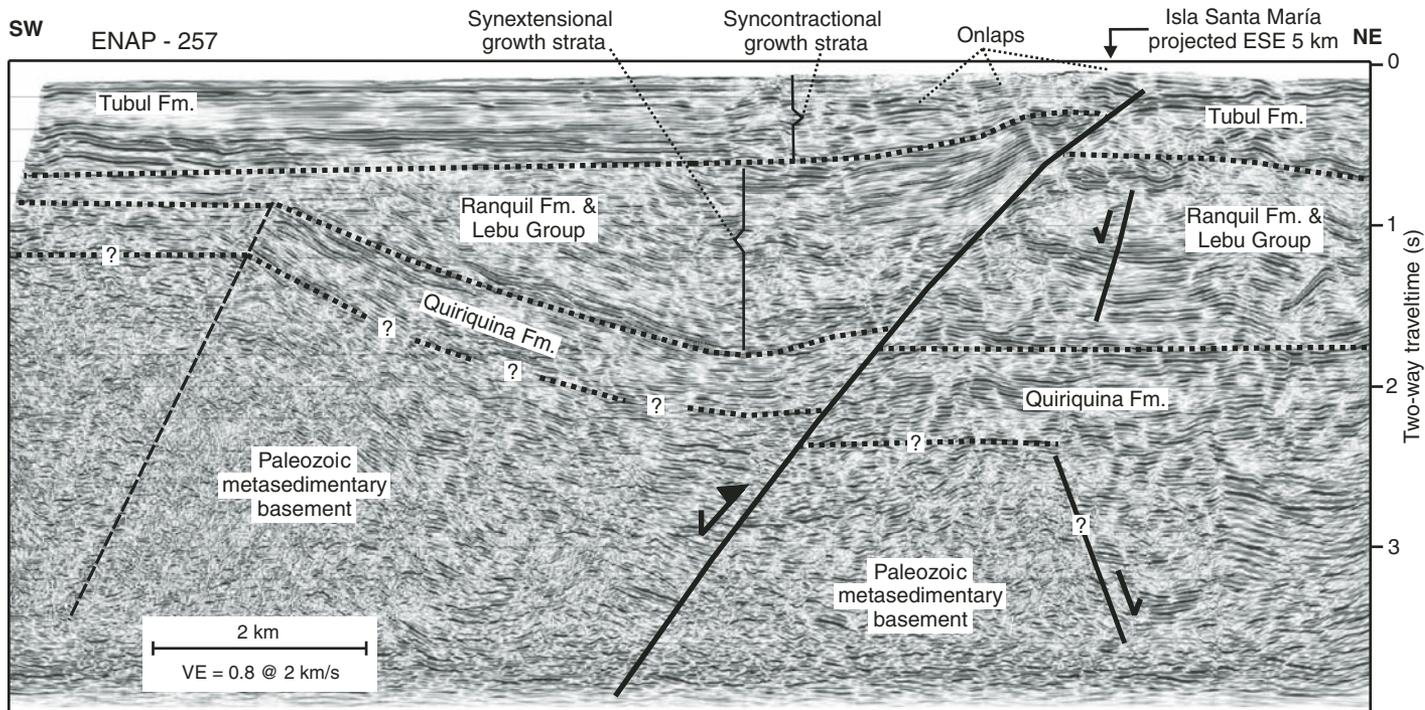
Figure 13. Reprocessed migrated seismic-reflection profile ENAP-257 (48-channel). See Figure 2C for location. Stratigraphy is correlated with nearby exploration boreholes. The synextensional Lebu Group and Ranquil Formation (Eocene to early Pliocene) were deposited in a half-graben controlled by a south-dipping normal fault. This fault was inverted between 3.6 and 2.5 Ma and has since controlled deposition of the syncontractional Tubul Formation. Note the increase in structural relief of the reverse-fault cored anticline below Isla Santa María between this profile and sections 016 and 259 (Figs. 11 and 12).

In contrast, the tilted and warped peninsulas and islands in the Arauco-Concepción area are narrow features, with wavelengths of less than 5 km, indicating that their emergence is instead dictated by the contractional reactivation of pre-existing steep normal faults imaged in seismic-reflection profiles.

Modern versus Millennial Uplift Rates

The earthquake-cycle model of subduction zones predicts inverse patterns during the interseismic strain accumulation and coseismic strain-release phases (Savage, 1983). This model, supported by geodetic measurements (e.g., Hyndman and Wang, 1995; Klotz et al., 2001), also predicts that most of the strain released during earthquakes is elastic and that only a small amount of permanent strain, which is the interseismic strain not recovered during coseismic deformation, accumulates after each cycle. The ~2 m/k.y. uplift rate calculated from the geological record for the last ~50 k.y. at Isla Santa María should thus represent the cumulative permanent strain averaged from many earthquake cycles.

At Isla Santa María, Darwin (1839) measured 2.4 to 3 m of coseismic uplift during the M ~ 8.25 earthquake in 1835 (Fig. 2B), but the abrasion platform uplifted during this earthquake is at the same elevation today (Fig. 4). The previous earthquake in 1751 is inferred to have had a larger magnitude of ~8.5 (Lomnitz, 2004). Coseismic uplift on the island during this event could have been ~6 m, judging by the elevation of a partially preserved abrasion platform above the 1835 surface (Fig. 4A). Therefore, these two surfaces should represent the permanent strain of the 1751 and 1835 cycles, implying a modern uplift rate that is over an order of magnitude higher than the millennial rate. This might indicate that the Concepción segment is neither slip- nor time-predictable,
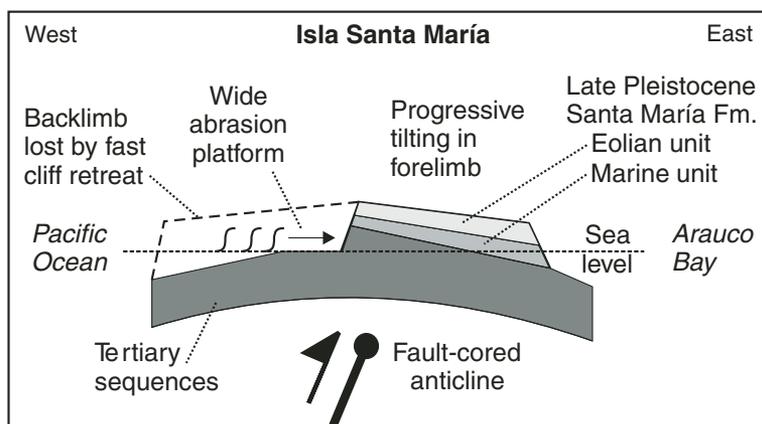

Figure 14. Schematic profile of Isla Santa María showing the relation between fault-cored anticline, progressive tilting and sedimentation in the forelimb, and backlimb removal by fast cliff retreat along the western coast exposed to the open Pacific Ocean

as has been shown for the Valdivia segment to the south (Cisternas et al., 2005).

Darwin noticed ~50% of postearthquake recovery at Talcahuano (Fig. 2B). This raises the question as to whether Isla Santa María also subsided after the earthquake, and subsequently emerged back to the same level or if it has remained at the same elevation since 1835. We cannot reconcile these issues with our data, but we can state that the island is slowly uplifting today in response to the seismically active reverse fault imaged below. In this region, GPS data show shortening, which has been inferred to be caused by locking of the plate interface (Klotz et al., 2001), and thus ongoing thrust-type shear of the upper plate by megathrust loading. Because no mega-earthquakes have ruptured the Concepción segment since 1835, loading there is expected to be in an advanced phase promoting thrust faulting and surface uplift.

CONCLUSIONS

The uplifting Isla Santa María was part of a submerged bedrock erosional platform at the edge of the Chilean shelf during the Pleistocene. Tectonic uplift and eustatic oscillations of sea level caused the onset of coastal marine sedimentation ca. 50 ka. Due to continuous tectonic uplift at ~2 m/k.y., the island emerged ca. 31 ka, and eolian sedimentary conditions prevailed. The eastward-inclined present-day surface of the island, the eastward increase in thickness of both the marine and eolian units of the late Pleistocene Santa María Formation, and a minimum of 20 emerged Holocene strandlines indicate progressive tilting at ~0.025°/k.y. during the late Quaternary.

Crustal seismicity and seismic-reflection profiles reveal active reverse faults, fault-cored anticlines, and growth strata that document ongoing shortening over the last 2.5 m.y. Deformation is distributed in folds and faults that individually accommodate low magnitudes of shortening. Focal mechanism solutions and the inclined alignment of crustal seismicity along a master fault indicate that it is rooted in the plate interface at ~12 km depth.

Isla Santa María is located at the intersection of two growing fault-cored anticlines; their lateral propagation produced progressive asymmetric tilting recorded in the Pleistocene marine and eolian units and the present-day surface of the island, which are growth strata in the forelimbs of both folds. Their backlimbs have been removed by cliff-retreat along the western side of the island, which is exposed to stronger erosion through waves from the open Pacific Ocean.

The highest coseismic uplift measured by Darwin during the 1835 earthquake is parallel to the seismogenic reverse fault system that extends from Isla Santa María across the Arauco Bay to the city of Concepción and surrounding areas. Importantly, this geometry suggests that blind reverse faults in the upper plate of a subduction zone can be triggered by great interplate earthquakes. In turn, these crustal faults control the distribution of low-wavelength surface features by folding of the upper crust between and probably also during interplate events. Consequently, subduction zone interplate earthquakes and upper-plate faults control the degree and areal extent of surface deformation, uplift, and associated seismic hazards. In the Arauco-Concepción area, active reverse faults result from inversion of Late Cretaceous to early Pliocene normal faults, and thus their inherited orientations control the geometry and distribution of emergent coastal landforms, emphasizing the fundamental role of inherited structures in seismotectonic segmentation of convergent margins.

REFERENCES CITED

Ando, M., 1975, Source mechanisms and tectonic significance of historical earthquakes along the Nankai Trough, Japan: Tectonophysics, v. 27, p. 119–140, doi: 10.1016/0040-1951(75)90102-X.

Angermann, D., Klotz, J., and Reiberg, C., 1999, Space-geodetic estimation of the Nazca–South American Euler vector: Earth and Planetary Science Letters, v. 171, p. 329–334, doi: 10.1016/S0012-821X(99)00173-9.

Bangs, N., and Cande, S.C., 1997, Episodic development of a convergent margin inferred from structures and processes along the southern Chile margin: Tectonics, v. 16, p. 489–503, doi: 10.1029/97TC00494.

Barnes, P.M., Nicol, A., and Harrison, T., 2002, Late Cenozoic evolution and earthquake potential of an active listric thrust complex above the Hikurangi subduction zone, New Zealand: Geological Society of America Bulletin, v. 114, p. 1379–1405, doi: 10.1130/0016-7606(2002)114<1379:LCEAEP>2.0.CO;2.

Barrientos, S., 1987, Is the Pichilemu-Talcahuano (Chile) a seismic gap?: Seismological Research Letters, v. 61, p. 43–48.

Beck, S., Barrientos, S., Kausel, E., and Reyes, M., 1998, Source characteristics of historic earthquakes along the Central Chile subduction zone: Journal of South American Earth Sciences, v. 11, p. 115–129, doi: 10.1016/S0895-9811(98)00005-4.

Berryman, K.R., 1993a, Age, height, and deformation of Holocene marine terraces at Mahia Peninsula, Hikurangi subduction margin, New Zealand: Tectonics, v. 12, p. 1347–1364.

Berryman, K.R., 1993b, Distribution, age, and deformation of late Pleistocene marine terraces at Mahia Peninsula, Hikurangi subduction margin, New Zealand: Tectonics, v. 12, p. 1365–1379.

Berryman, K.R., Ota, Y., and Hull, A.G., 1989, Holocene paleoseismicity in the fold and thrust belt of the Hikurangi subduction zone, eastern North Island, New Zealand: Tectonophysics, v. 163, p. 185–195, doi: 10.1016/0040-1951(89)90256-4.

Biró, L., 1979, Contribución al conocimiento de la Formación Tubul, Plioceno Superior, Provincia de Arauco (37°14′S): II Congreso Geológico Chileno: Arica, Chile, Sociedad Geológica de Chile, p. H33–H44.

Bohm, M., Lüth, S., Echtler, H., Asch, G., Bataille, K., Bruhn, C., Rietbrock, A., and Wigger, P., 2002, The Southern Andes between 36°S and 40°S latitude: Seismicity and average velocities: Tectonophysics, v. 356, p. 275–289, doi: 10.1016/S0040-1951(02)00399-2.

Bookhagen, B., Echtler, H., Melnick, D., and Strecker, M., 2005, Holocene tectonic coastal uplift and tilting constrain through surface deformation on Santa María Island, south-central Chile active margin: Salt Lake City, Utah, Geological Society of America Abstracts with Programs, v. 37, no. 7, paper 149-13.

Bookhagen, B., Echtler, H.P., Melnick, D., Strecker, M.R., and Spencer, J.Q.G., 2006, Using uplifted Holocene beach berms for paleoseismic analysis on the Santa María Island, south-central Chile: Geophysical Research Letters, v. 10.1029/2006GL026734.

Briggs, R.W., Sieh, K., Meltzner, A.J., Natawidjaja, D., Galetzka, J., Suwargadi, B., Hsu, Y.-J., Simons, M., Hananto, N., Suprihanto, I., Prayudi, D., Avouac, J.-P., Prawirodirdjo, L., and Bock, Y., 2006, Deformation and slip along the Sunda megathrust in the great 2005 Nias-Simeulue earthquake: Science, v. 311, p. 1897–1901, doi: 10.1126/science.1122602.

Bruhn, C., 2003, Momententensoren hochfrequenter Ereignisse in Sudchile [Ph.D. thesis]: Potsdam, University of Potsdam, 181 p.

Bruhn, R.L., and Haeussler, P.J., 2006, Deformation driven by subduction and microplate collision: Geodynamics of Cook Inlet basin, Alaska: Geological Society of America Bulletin, v. 118, p. 289–303, doi: 10.1130/B25672.1.

Campos, J., Hatzfeld, D., Madariaga, R., López, G., Kausel, E., Zollo, A., Iannacone, G., Fromm, R., Barrientos, S., and Lyon-Caen, H., 2002, A seismological study of the 1835 seismic gap in south-central Chile: Physics of the Earth and Planetary Interiors, v. 132, p. 177–195, doi: 10.1016/S0031-9201(02)00051-1.

Carr, A.S., Thomas, D.S.G., and Bateman, M.D., 2006, Climatic and sea level controls on Late Quaternary eolian activity on the Agulhas Plain, South Africa: Quaternary Research, v. 65, p. 252–263, doi: 10.1016/j.yqres.2005.10.001.

Cifuentes, I.L., 1989, The 1960 Chilean earthquake: Journal of Geophysical Research, v. 94, p. 665–680.

Cisternas, M., Atwater, B.F., Torrejón, F., Sawai, Y., Machuca, G., Lagos, M., Eipert, A., Youlton, C., Salgado, I., Kamataki, T., Shishikura, M., Rajendran, C.P., Malik, J.K., Rizal, Y., and Husni, M., 2005, Predecessors of the giant 1960 Chile earthquake: Nature, v. 437, p. 404–407, doi: 10.1038/nature03943.

Comte, D., Eisenberg, A., Lorca, E., Pardo, M., Ponce, L., Saragoni, R., Singh, S., and Suárez, G., 1986, The 1985 central Chile earthquake, a repeat of previous earthquakes in the region?: Science, v. 233, p. 449–453.

Darwin, C., 1839, Journal and remarks, 1832–1836, *in* Colburn, H., ed., Narrative of the surveying voyages of His Majesty's ships *Adventure* and *Beagle* between the years 1826 and 1836, describing their examination of the southern shores of South America, and the *Beagle*'s circumnavigation of the globe: London, UK; reprint 1966, New York, USA, Abrahams Magazine Service (AMS) Press, v. 3, p. 370–381.

Darwin, C., 1851, Geological observations of South America, geological observations on coral reefs, volcanic islands and on South America—Being the voyage of the *Beagle*, under the Command of Captain Fitzroy, R.N., during the years 1832 to 1836: London, Smith and Elder, 279 p.

Elgueta, S., and Arcos, R., 1994, Geología y modelo de sedimentación de la secuencia Cretácico Terciaria de la Cuenca de Arauco [Geology and sedimentation model of the Cretaceous-Tertiary sequence of the Arauco Basin]: Santiago, Chile, Empresa nacional del Petróleo, 34 p.

Finger, K., Nielsen, S., DeVries, T., Encinas, A., and Peterson, D., 2006, Paleontologic evidence for sedimentary displacement in Neogene forearc basins of central Chile: Palaios (in press).

FitzRoy, R., 1839, Proceedings of the second expedition, 1831–1836, under the command of Captain Robert FitzRoy, *in* Colburn, H., ed., Narrative of the surveying voyages of His Majesty's ships *Adventure* and *Beagle* between the years 1826 and 1836, describing their examination of the southern shores of South America, and the *Beagle*'s circumnavigation of the globe: London, UK; reprint 1966, New York, USA, Abrahams Magazine Service (AMS) Press, 695 p.

Glodny, J., Lohrmann, J., Echtler, H., Gräfe, K., Seifert, W., Collao, S., and Figueroa, O., 2005, Internal dynamics of a paleoaccretionary wedge: Insights from combined isotope tectonochronology and sandbox modelling of the south-central Chilean forearc: Earth and Planetary Science Letters, v. 231, no. 1–2, p. 23–39, doi: 10.1016/j.epsl.2004.12.014.

Goldfinger, C., Kulm, L.D., Yeats, R.S., Appelgate, B., Mackay, M.E., and Moore, G.F., 1992, Transverse structural trends along the Oregon convergent margin: Implications for Cascadia earthquake potential and crustal rotations: Geology, v. 20, p. 141–144, doi: 10.1130/0091-7613(1992)020<0141:TSTATO>2.3.CO;2.

González, E., 1989, Hydrocarbon resources in the coastal zone of Chile, *in* Ericksen, G.E., Cañas Pinochet, M.T., and Reinemund, J.A., eds., Geology of the Andes and its relation to hydrocarbon and mineral resources: Houston, Texas, Circum-Pacific Council for Energy and Mineral Resources, p. 383–404.

Grevemeyer, I., Díaz-Naveas, J.L., Ranero, C.R., and Villinger, H.W., 2003, Heat flow over the descending Nazca plate in central Chile, 32°S to 41°S: Observations from ODP Leg 202 and the occurrence of natural gas hydrates: Earth and Planetary Science Letters, v. 213, p. 285–298, doi: 10.1016/S0012-821X(03)00303-0.

Hughen, K., Herring, C., Marchal, O., Lehman, S., Turnbull, J., Southon, J., and Overpeck, J., 2004, ^{14}C Activity and global carbon cycle changes over the past 50,000 years: Science, v. 303, p. 202–207, doi: 10.1126/science.1090300.

Hyndman, R.D., and Wang, K., 1995, The rupture zone of Cascadia great earthquakes from current deformation and the thermal regime: Journal of Geophysical Research, v. 100, p. 22,133–22,154, doi: 10.1029/95JB01970.

Johnson, S.Y., Blakely, R.J., Stephenson, W.J., Dadisman, S.V., and Fisher, M.A., 2004, Active shortening of the Cascadia forearc and implications for seismic hazards of the Puget Lowland: Tectonics, v. 23, p. TC1011, doi: 10.1029/2003TC001507.

Kaizuka, S., Matsuda, T., Nogami, M., and Yonekura, N., 1973, Quaternary tectonic and recent seismic crustal movements in the Arauco Peninsula and its environs, central Chile: Geographical Reports Tokyo Metropolitan University, v. 8, p. 1–49.

Kanamori, H., 1977, The energy release in great earthquakes: Journal of Geophysical Research, v. 82, p. 2981–2987.

Kelleher, J.A., 1972, Rupture zones of large South American earthquakes and some predictions: Journal of Geophysical Research, v. 77, p. 2089–2103.

Klotz, J., Khazaradze, G., Angermann, D., Reigber, C., Perdomo, R., and Cifuentes, O., 2001, Earthquake cycle dominates contemporary crustal deformation in central and southern Andes: Earth and Planetary Science Letters, v. 193, p. 437–446, doi: 10.1016/S0012-821X(01)00532-5.

Krawczyk, C., and the SPOC (Subduction Processes Off Chile) team, 2003, Amphibious seismic survey images plate interface at 1960 Chile earthquake: Eos (Transactions, American Geophysical Union), v. 84, p. 304–305.

Le Roux, J.P., and Elgueta, S., 1997, Paralic parasequences associated with Eocene sea-level oscillations in an active margin setting: Trihueco Formation of the Arauco Basin, Chile: Sedimentary Geology, v. 110, p. 257–276, doi: 10.1016/S0037-0738(96)00086-3.

Lohrmann, J., 2002, Identification of parameters controlling the accretive and tectonically erosive mass-transfer mode at the south-central and north Chilean forearc using scaled 2D sandbox experiments [Ph.D. thesis]: Berlin, Freie University, 236 p.

Lomnitz, C., 1970, Major earthquakes and tsunamis in Chile during the period 1535 to 1955: Geologische Rundschau, v. 59, p. 938–960, doi: 10.1007/BF02042278.

Lomnitz, C., 2004, Major earthquakes of Chile: A historical survey, 1535–1960: Seismological Research Letters, v. 75, p. 368–378.

Matsuda, T., Ota, Y., Ando, M., and Yonekura, N., 1978, Fault mechanism and recurrence time of major earthquakes in southern Kanto district, Japan, as deduced from coastal terrace data: Geological Society of America Bulletin, v. 89, p. 1610–1618, doi: 10.1130/0016-7606(1978)89<1610:FMARTO>2.0.CO;2.

Melnick, D., and Echtler, H.P., 2006, Inversion of forearc basins in south-central Chile caused by rapid glacial age trench fill: Geology, v. 34, doi: 10.1130/G22440.1.

Mordojovich, C., 1981, Sedimentary basins of Chilean Pacific offshore, *in* Halbouty, M.T., ed., Energy resources of the Pacific region: American Association of Petroleum Geologists, Studies in Geology, v. 12, p. 63–82.

Mpodozis, C., and Ramos, V., 1989, The Andes of Chile and Argentina, *in* Ericksen, G.E., Cañas Pinochet, M.T., and Reinemund, J.A., eds., Geology of the Andes and its relation to hydrocarbon and mineral resources: Houston, Texas, Circum-Pacific Council for Energy and Mineral Resources, p. 59–90.

Muñoz-Cristi, J., 1946, Estado actual del conocimiento sobre la geología de la provincia de Arauco: Anales Universidad de Chile, v. 3, p. 30–63.

Nelson, R., and Manley, W., 1992, Holocene coseismic and aseismic uplift of the Isla Mocha, south-central Chile: Quaternary International, v. 15/16, p. 61–76, doi: 10.1016/1040-6182(92)90036-2.

Nishenko, S., 1985, Seismic potential for large and great interplate earthquakes along the Chilean and southern Peruvian margins of South America: A quantitative reappraisal: Journal of Geophysical Research, v. 90, p. 3589–3615.

Ota, Y., and Yamaguchi, M., 2004, Holocene coastal uplift in the western Pacific Rim in the context of late Quaternary uplift: Quaternary International, v. 120, p. 105–117, doi: 10.1016/j.quaint.2004.01.010.

Pandolfi, M., Best, M.R., and Murray, S.P., 1994, Coseismic event of May 15, 1992, Huon Peninsula, Papua New Guinea: Geology, v. 22, p. 239–240, doi: 10.1130/0091-7613(1994)022<0239:CEOMHP>2.3.CO;2.

Park, J.O., Tsuru, T., Kodaira, S., Nakanishi, A., Miura, S., Kaneda, Y., and Kono, Y., 2000, Out-of-sequence thrust faults developed in the coseismic slip zone of the 1946 Nankai earthquake (Mw=8.2) off Shikoku, southwest Japan: Geophysical Research Letters, v. 27, p. 1033–1036, doi: 10.1029/1999GL008443.

Paskoff, R., and Manríquez, H., 2004, Las dunas de las costas de Chile [The dunes of the coasts of Chile]: Santiago, Instituto Geográfico Militar, 113 p.

Philip, H., and Meghraoui, M., 1983, Structural analysis and interpretation of the surface deformation during El Asnam earthquake of October 10, 1980: Tectonics, v. 2, p. 17–49.

Pineda, V., 1986, Evolución paleográfica de la cuenca sedimentaria Cretácico-Terciaria de Arauco, *in* Frutos, J., Oyarzún, R., and Pincheira, M., eds., Geología y recursos minerales de Chile: Concepción, Universidad de Concepción, p. 375–390.

Pineda, V., 1999, El cañón submarino del Bío-Bío: Aspectos dinámicos y ambientales [Ph.D. thesis]: Concepción, Universidad de Concepción, 151 p.

Plafker, G., 1972, Alaskan earthquake of 1964 and Chilean earthquake of 1960—Implications for arc tectonics: Journal of Geophysical Research, v. 77, p. 901–925.

Plafker, G., and Savage, J.C., 1970, Mechanism of the Chilean earthquake of May 21 and 22, 1960: Geological Society of America Bulletin, v. 81, p. 1001–1030.

Rabassa, J., and Clapperton, C.M., 1990, Quaternary glaciations of the southern Andes: Quaternary Science Reviews, v. 9, p. 153–174, doi: 10.1016/0277-3791(90)90016-4.

Reichert, C., Schreckenberger, B., and the SPOC team, 2002, Cruise Report SONNE SO-161 Leg 2&3 SPOC—Subduction Processes Off Chile, BMBF—Forschungsvorhaben 03G0161A: Hannover, Germany, Federal Institute for Geosciences and Natural Resources (BGR), 154 p.

Rietbrock, A., Haberland, C., Bataille, K., Dahm, T., and Oncken, O., 2005, Studying the seismogenic coupling zone with a passive seismic array: Eos (Transactions, American Geophysical Union), v. 86, p. 293.

Rodríguez, S., 1835, Informe presentado a la intendencia de la Provincia de Concepción de Chile, por Ambrosio Lozier, Simón Rodríguez y Juan José Arteaga, nombrados para reconocer la ciudad de Concepción y sus cercanías, después del terremoto de 20 Febrero de 1835, *in* Simón, Rodríguez, Obras completas 1975: Caracas, Venezuela, Universidad Simón Rodríguez, v. 1, p. 471–507.

Savage, J.C., 1983, A dislocation model of strain accumulation and release at a subduction zone: Journal of Geophysical Research, v. 88, p. 4984–4996.

Siddall, M., Rohling, E.J., Almogi-Labin, A., Hemleben, C., Meischner, D., Schmelzer, I., and Smeed, D.A., 2003, Sea-level fluctuations during the last glacial cycle: Nature, v. 423, p. 853–858, doi: 10.1038/nature01690.

Somoza, R., 1998, Updated Nazca (Farallon)–South American relative motions during the last 40 My: Implications for mountain building in the Andes: Journal of South American Earth Sciences, v. 11, p. 211–215, doi: 10.1016/S0895-9811(98)00012-1.

Stewart, I.S., Sauber, J., and Rose, J., 2000, Glacio-seismotectonics: Ice sheets, crustal deformation and seismicity: Quaternary Science Reviews, v. 19, p. 1367–1389, doi: 10.1016/S0277-3791(00)00094-9.

Stuiver, M., Reimer, P.J., Bard, E., Beck, J.W., Burr, G.S., Hughen, K.A., Kromer, B., McCormac, G., Van Der Plicht, J., and Spurk, M., 1998, INTCAL98 radiocarbon age calibration, 24,000–0 cal BP: Radiocarbon, v. 40, p. 1041–1083.

Suppe, J., Chou, G.T., and Hook, S.C., 1992, Rates of folding and faulting determined from growth strata, *in* McClay, K.R., ed., Thrust tectonics: New York, Chapman and Hall, p. 105–121.

Taylor, F., Frohlich, C., Lecolle, J., and Strecker, M., 1987, Analysis of partially emerged corals and reef terraces in the central Vanuatu Arc: Comparison of contemporary coseismic and nonseismic with Quaternary vertical movements: Journal of Geophysical Research, v. 92, p. 4905–4933.

Tebbens, S.F., and Cande, S.C., 1997, Southeast Pacific tectonic evolution from early Oligocene to present: Journal of Geophysical Research, v. 102, p. 12,061–12,084, doi: 10.1029/96JB02582.

Thatcher, W., 1990, Order and diversity in modes of circum-Pacific earthquake recurrence: Journal of Geophysical Research, v. 95, p. 2609–2624.

Vietyes, H., Arcos, R., and González, A., 1993, Interpretación geológica de sísmica marina del Golfo de Arauco [Geological interpretation of marine seismics from the Arauco Gulf]: Santiago, Chile, Empresa nacional del Petróleo, 17 p.